Transcriptional characterization of subcutaneous adipose tissue in obesity affected women highlights metabolic dysfunction and implications for lncRNAs

Federica Rey, Letizia Messa, Cecilia Pandini, Bianca Barzaghini, Giancarlo Micheletto, Manuela Teresa Raimondi, Simona Bertoli, Cristina Cereda, Gian Vincenzo Zuccotti, Raffaella Cancello, Stephana Carelli

PII: S0888-7543(21)00356-6

DOI: https://doi.org/10.1016/j.ygeno.2021.09.014

Reference: YGENO 10179

To appear in: *Genomics*

Received date: 18 May 2021

Revised date: 3 September 2021

Accepted date: 17 September 2021

Please cite this article as: F. Rey, L. Messa, C. Pandini, et al., Transcriptional characterization of subcutaneous adipose tissue in obesity affected women highlights metabolic dysfunction and implications for lncRNAs, *Genomics* (2018), https://doi.org/10.1016/j.ygeno.2021.09.014

Transcriptional characterization of Subcutaneous Adipose Tissue in obesity affected women highlights metabolic dysfunction and implications for lncRNAs

Federica Rey[1,2,*], Letizia Messa[3,*], Cecilia Pandini[4], Bianca Barzaghini[3], Giancarlo Micheletto[5], Manuela Teresa Raimondi[3], Simona Bertoli[6,7], Cristina Cereda[4,^], Gian Vincenzo Zuccotti[1,2,8], Raffaella Cancello[6,$], Stephana Carelli[1,2,$,°]

[1] Department of Biomedical and Clinical Sciences "L. Sacco", University of Milan, Via Grassi 74, 20157 Milan, Italy

[2] Pediatric Clinical Research Centre Fondazione "Romeo ed Enrica Invernizzi", University of Milano, Milano, Italy

[3] Department of Chemistry, Materials and Chemical Engineering "Giulio Natta", Politecnico di Milano, Milano, Italy

[4] Genomic and post-Genomic Centre, IRCCS Mondino Foundation, 27100 Pavia, Italy

[5] Department of Pathophysiology and Transplantation, INCO and Department of General Surgery, Istituto Clinico Sant'Ambrogio, University of Milan, Milan, Italy

[6] Obesity Unit—Laboratory of Nutrition and Obesity Research, Department of Endocrine and Metabolic Diseases, IRCCS Istituto Auxologico Italiano, Milan, Italy

[7] International Center for the Assessment of Nutritional Status (ICANS), Department of Food, Environmental and Nutritional Sciences (DeFENS), University of Milan, Milan, Italy

[8] Department of Pediatrics, Children's Hospital "V. Buzzi", Milan, Italy

[^] Present address: Cristina Cereda, Department of Women, Mothers and Neonatal Care, Children's Hospital "V. Buzzi", Milan, Italy mail: cristina.cereda@asst-fbf-sacco.it

[*] These authors contributed equally to the work.

[$] These authors contributed equally to the work.

[°] Please address all correspondence to Dr. Stephana Carelli, stephana.carelli@unimi.it, Pediatric Clinical Research Center Fondazione "Romeo ed Enrica Invernizzi", University of Milano, Milano, Italy

Keywords: obesity, transcriptome, RNA-seq, lncRNAs, gene expression, metabolic diseases

Abstract

Obesity is a complex disease with multifactorial causes, and its prevalence is becoming a serious health crisis. For this reason, there is a crucial need to identify novel targets and players. With this aim in mind, we analyzed via RNA-sequencing the subcutaneous adipose tissue of normal weight and obesity-affected women, highlighting the differential expression in the two tissues. We specifically focused on long non-coding RNAs, as 6 of these emerged as dysregulated in the diseased-tissue (COL4A2-AS2, RPS21-AS, PELATON, ITGB2-AS1, ACER2-AS and CTEPHA1). For each of them, we performed both a through *in silico* dissection and *in vitro* validation, to predict their function during adipogenesis. We report the lncRNAs expression during adipose derived stem cells differentiation to adipocytes as model of adipogenesis and their potential modulation by adipogenesis-related transcription factors (C/EBPs and PPARγ). Moreover, inhibiting CTEPHA1 expression we investigated its impact on adipogenesis-related transcription factors, showing its significative dysregulation of C/EBPα expression. Lastly, we dissected the subcellular localization, pathway involvement and disease-correlation for coding differentially expressed genes. Together, these findings highlight a transcriptional deregulation at the basis of obesity, impacted by both coding and long non-coding RNAs.

Introduction

Obesity is defined as abnormal or excessive fat accumulation, presenting a risk to health (1). The most recent update of the World Health Organization (WHO) reports how the worldwide prevalence of obesity nearly tripled between 1975 and 2016, with over 650 million adults being clinically defined as obese (1). The most significant implication is the increased risk of co-morbidities development, such as type 2 diabetes (T2D), hypertension, dyslipidemia, coronary artery disease, stroke, osteoarthritis and even certain forms of cancer increasing mortality and direct and indirect socioeconomic costs (1-4). Canonical approaches to counteract obesity involve decreasing energy intake by choosing a suitable diet and increasing the energy expenditure with exercise, but these two approaches alone are not always sufficient (5). There is thus a need to identify and characterize novel implicated targets, in order to identify new regulators in disease pathogenesis along with novel potential therapeutic targets. The identification of genes implicated in the obesity development has been possible thanks to Genome Wide Association Studies, which have allowed the identification of mutations and polymorphisms which can be associated to BMI increase, waist circumference, and waist-to-hip ratio (6). To date, more than 97 loci related to complex obesity that account for approximately 2.7% of BMI, waist circumference, and waist-to-hip ratio variations have been identified (6). Even so, it is not possible to claim that obesity can be caused either by the genes or the environment, but it is rather possible to state that behavior and genes are different levels of the same causal framework (7-9). In this context, epigenetic aspects need to be considered as they are crucial regulators in the translation of environment stimuli on gene expression regulation (7-9).

In recent years, the role of transcriptome is always taking on prominence and its relevance in the regulation of biologic processes is now reconsidered since up to 90% of the genome is transcribed and not translated into a protein (10). Among the epigenetic modulators there are

also small non-coding RNAs, which include micro RNAs (miRNA), and long non-coding RNAs (lncRNAs), subdivided according to their dimension (10). These transcripts are relevant also in the field of adipogenesis, fat mass expansion and obesity. High throughput screening have allowed for the identification of novel targets, at both coding and non-coding levels. Proteomics studies have been performed highlighting deregulated proteins in adipose tissue of obesity-affected patients (11). Moreover, miRNAs have been found to play regulatory roles in adipose tissue and obesity (12). Specifically, there are also increasing evidence of the role of lncRNAs in adipogenesis, where their expression levels correlate with different stages of adipocytes differentiation, they can regulate key players in adipogenesis (e.g., PPARγ), or even associate with adipogenesis-implicated miRNAs (13, 14). Moreover, RNA-seq screening allowed to the identification of deregulated targets in patients with obesity or murine models of obesity (15, 16). These studies have been performed in both brown and white adipose tissue, providing reference of a number of adipogenesis-related lncRNAs (15, 17). Hence, lncRNAs are emerging as new potential candidate targets for therapeutic development as well as comorbidities regulators (16, 18-21).

In this framework, the aim of this work was the characterization of transcriptional differences in the subcutaneous adipose tissue of obesity-affected versus normal weight healthy women. We previously highlighted the presence of different transcriptional profiles in obesity-affected men and women, highlighting gender-specific differences in transcription, and we also performed a characterization of the oncogenic susceptibility present in SAT tissues of normal weight subject, obesity-affected women, obesity and type 2 diabetes-affected women and obesity-affected men (4, 22). We now aim to perform an in-depth characterization of coding and non-coding transcripts in obesity affected women versus healthy women, specifically focusing on role of the deregulated lncRNAs. Here we investigate a panel of them (n=6) in terms of expression and regulation in human Adipose Derived Stem Cells (hADSCs) differentiation to adipocytes.

Materials and Methods

Adult human adipose tissue collection, isolation and differentiation

The present study is in accordance with the Declaration of Helsinki, and it was approved by the Ethical Committee of IRCCS Istituto Auxologico Italiano (Ethical Committee approval code #2020_10_20_04). A signed informed consent was obtained from each enrolled patient for tissue sampling. Biopsies of SAT were collected from a total of 10 subjects: 5 healthy CTRL women (age 37 ± 6.7 years, BMI 24.3 ± 0.9 kg/m2) and 5 women with obesity (age 41 ± 12.5 years, BMI 38.2 ± 4.6 kg/m2). Patients were chosen so not to have significant differences amongst groups which could impact on gene expression (Table S1). Surgical biopsies of whole abdominal subcutaneous adipose tissues (SAT) were collected pre-operatively from obese patients during bariatric surgery procedures and from CTRL women before aesthetic plastic surgery or abdominal surgery for non-inflammatory diseases. Each collected biopsy was weighed and stored in 1 ml of DMEM (Invitrogen Corporation, Jefferson City, MO) supplemented with 2.5% Bovine Serum Albumin (Sigma, St. Louis, MO) per gram of collected tissue. The biopsy was immediately transferred to the laboratory and processed. A fragment of the whole adipose tissue biopsy was immediately frozen in liquid

nitrogen for RNA extraction (see below), another fragment was formalin-fixed, and the remaining material was digested with 1 mg/ml collagenase type 2 (Sigma, St. Louis, MO) for at least 1 h at 37°C under shaking. The digested tissue was then filtered through a sterile gauze and a nylon filter (BD Bioscience 1 Becton Drive Franklin Lakes, NJ). The SVF cells were isolated by centrifugation and then treated with a buffer containing 154 mM NH4Cl, 10 mM KHCO3, and 0.1 mM EDTA for lysis of red blood cells. Stroma-Vascular Fraction cells were plated and cultured in a medium containing a 1:1 mixture of Ham's F12/DMEM (Invitrogen Corporation, Jefferson City, MO) supplemented with 10% Fetal Bovine Serum (FBS, Sigma, St. Louis, MO) until confluence. The cells obtained have been identified to be human Adipose Derived Stem Cells (23). At confluence, cells were differentiated into mature adipocytes using AdipoStemPro (Invitrogen) for 10 days.

SAT RNA extraction

Approximately 500 mg of frozen SAT was homogenized in RLT buffer (Qiagen). RNA from SAT was extracted using the RNeasy Mini Kit (Qiagen) according to the manufacturer protocol and samples were then treated with the RNase-Free DNase Set (Qiagen). Concentration and quality of the extracted RNA were determined by the NanoDrop ND-1000 spectrophotometer (NanoDrop Technologies, USA) and RNA integrity verified by gel-electrophoresis.

RNA-Seq and bioinformatic data analysis

RNA-seq analysis was performed on one replicate for each SAT biopsy (5 healthy CTRL women and 5 women with obesity). RNA-seq libraries were prepared with the CORALL Total RNA-Seq Library Prep Kit (Lexogen, Vienna, Austria) using 150 ng total RNAs. The RiboCop rRNA Depletion Kit (Lexogen, Vienna, Austria) was used to remove rRNA. Qualities of sequencing libraries were assessed with D1000 ScreenTape Assay using the 4200 TapeStation System (Agilent, Santa Clara, CA, USA) to account for variability in library quality and quantified with Qubit™ dsDNA HS Assay Kit (Invitrogen, Carlsbad, CA, USA). To account for technical variability in library dimension the single libraries were normalized for their molarity using the respective "library quantification file" (Lexogen, Vienna, Austria) which calculates the molarities of each library from the concentration measurement and average size, providing the volumes of each library to be used for preparation of an equimolar lane mix.

RNA processing was carried out using Illumina NextSeq 500 Sequencing. FastQ files were generated via llumina bcl2fastq2 (v. 2.17.1.14; https://support.illumina.com/downloads/bcl2fastq-conversion-software-v2-20.html, last accessed on 15 February 2021) starting from raw sequencing reads produced by Illumina NextSeq sequencer. Quality of individual sequences was evaluated using FastQC software (see Code Availability 1) after adapter trimming with cutadapt software. Transcript abundance was obtained using the BlueBee® Genomics Platform (Lexogen, Vienna, Austria) using Gencode Release h38 (GRCh38) as a reference. Differential expression analysis was performed using R package DESeq2, which contains a further library normalization step. Genes were considered differentially expressed and retained for further analysis with $|\log2(\text{condition sample/control sample})| \geq 1$ and a False Discovery Rate (FDR) ≤ 0.1. The raw

data obtained from the RNA-seq analysis are deposited in the Gene Expression Omnibus repository with the accession number GSE166047. The expression of a panel of genes with relevant FC differences was previously analyzed via Real-Time PCR in technical duplicates in an independent cohort of SAT samples obtained from normal-weight females and females affected by obesity. This accounts for technical and inter-individual differences (4).

Pathway analysis

Gene set enrichment analysis was performed on clusterProfiler R package (24). Gene set from Molecular Signature databases such as curated gene set (C2) and ontology gene sets (C5) and a p value cut off < 0.05 were considered for this analysis (24). The R software was used to generate heatmaps (*heatmap.2* function from the R *ggplots* package), PCA plot (*prcomp* function from the R *ggplots* package), and Volcano plots (25). The NDEx plugin (26) was used to perform analysis regarding the subcellular localization of the differentially expressed genes (27).

Coding and ncRNAs co-expression analysis

Coding RNAs' co-expression with ncRNAs was performed using Weighted gene co-expression network analysis (WGCNA) R package (https://CRAN.R-project.org/package=WGCNA) (28). The soft thresholding power was chosen considering the criterion of approximate scale-free topology. Network nodes represent gene expression profiles, while undirected edges values are the pairwise correlations between gene expressions. Cytoscape software was used for network import and visualization.

***In silico* dissection of lncRNAs**

The AnnoLnc2 database was used for characterization of each lncRNA (29). The FASTA sequence for each lncRNA was submitted to the website, which retrieved information on the lncRNAs localization, repeat elements analysis through the RepeatMasker genomic datasets, sequence conservation with PhyloP, PhastCons scores and Derived Allele Frequency (DAF) scores, lncRNAs expression, localization, and localization motifs. The secondary structure prediction was used for the identification of miRNA and protein binding sites (identified via CLIP-Seq). Moreover, AnnoLnc2 through GTRD database allowed to highlight peak clusters of transcription factors (TFs) in adipocytes, and we also cross-referenced all the genes which emerged as positively correlated with each lncRNA with the DE RNAs from our RNA-seq analysis. Amongst these, we searched for cis/trans correlations with the LncEXPdb (30) interaction section. Lastly, we investigated the biological processes positively correlated with the AnnoLnc2 database and we report the top 20 significant pathways.

hADSCs' isolation

Primary cell cultures from normal weight human adipose tissue samples were obtained from one volunteer healthy subject undergoing elective liposuction procedures under local anesthesia. Briefly, cells were isolated after directly plating the pellet without centrifugation in complete DMEM prepared with DMEM (Euro Clone) containing 1g/l D-glucose 10% heat-inactivated FBS supplemented with antibiotics at 37°C in a humidified, 5% CO_2 incubator (HERA cell 150- Thermo electron, USA). The obtained cells were characterized for their

karyotype and immunophenotype (31, 32). All cell cultures were maintained at 37°C in humidified atmosphere containing 5% CO_2. After 2 weeks, the non-adherent fraction was removed and the adherent cells were cultured continuously, while the medium was changed every 3 days.

Adipogenic induction

hADSCs were differentiated in adipogenic medium composed of DMEM High Glucose (Euroclone) supplemented with 10% Fetal Bovine Serum (GIBCO™), antibiotics (1% Penicillin/Streptomycin, 0.3% Amphotericin B) (Euroclone), 1% L-Glutamine (Euroclone), 1 μmol/L dexamethasone (Sigma-Aldrich), 0.5 mM 3-isobutyl-1-methyl-xanthine (Sigma-Aldrich), 10 μM insulin (Sigma-Aldrich) and 200 μM indomethacin (Sigma-Aldrich). The medium was changed every 3 days. In the experiments showed in this work adipogenic induction required 7 days (31, 33, 34), but time-point experiments were also conducted assessing adipogenic differentiation at different days.

Pharmacological treatments

PPARγ was activated using the ligand agonist troglitazone (35, 36). 1 μg/mL troglitazone (Sigma-Aldrich) was added to the standard culture medium with 10% FBS for 7 days, and medium was changed every 2 days. PPARγ was inhibited with the selective PPARγ antagonist T0070907 (Sigma-Aldrich)(37). 1 μM of T0070907 was added to the standard culture medium for 7 days, and the medium was changed every 2 days (34).

Gene expression silencing

RNA interference was used to suppress specific gene expression. Briefly, two days before transfection, 6,000 cells/cm^2 were plated in standard growth medium. Transfection was performed with Lipofectamine® RNAiMAX Reagent (Thermo Fisher) and siRNA agent. This was a siRNA mock (Silencer™ Select Negative Control No. 1 siRNA-Cat # 4390843, Thermo Fisher) or the siRNA for the respective target (Silencer Select pre-designed siRNA for C/EBPα - s532363, C/EBPδ - s2894, C/EBPβ - s63860 and CTEPHA1 - n360183; Thermo Fisher) diluted in the appropriate volume of Opti-MEM® Medium (Thermo Fisher). Samples were incubated for <15 minutes at room temperature and the siRNA-lipid complex was gently dropped in the wells containing the cells, which were then incubated for 72h days at 37°C in a CO_2 incubator.

Real Time PCR

Total RNA was isolated using TRIzol Reagent ™ (Invitrogen) in accordance with manufacturer's instructions. 500 ng of RNA were reverse transcribed using the iScript ™ Reverse Transcription Supermix for RT-qPCR (Bio-Rad). Real Time PCR was performed with StepOnePlus™ Real Time PCR System (Thermo Fisher) using Sso SYBR Green Supermix (Bio-Rad). Samples were analyzed with the $2^{-\Delta\Delta Ct}$ method, where $\Delta\Delta Ct = \Delta Ct$ sample – ΔCt reference (38).Primers were designed using human gene sequences available from NCBI (www.ncbi.nlm.nih.gov/nucleotide), and selected using NCBI's Primer- BLAST tool at the exon junctions' level to optimize amplification from RNA templates and avoiding nonspecific amplification products. Primers were designed to have a sequence of about 20 bp

and perform a PCR product size of maximum 250 bp. 18S and GAPDH were used as housekeeping genes. Primer used are shown in Table S2.

Statistical analysis

Statistics was evaluated using GraphPad Prism 8.0a version (GraphPad Software Inc, La Jolla, USA). When two conditions were analyzed, Student's unpaired t test was used. When three or more conditions were analyzed, one-way ANOVA was used followed by Tukey's post-test. For all in vitro experiments, data are reported as mean ± Standard Error Mean (SEM). The level of statistical significance was set at p=0.05.

Results

Obesity alters expression profiles of coding and non-coding genes in SAT

Subcutaneous adipose tissue (SAT) from 5 normal weight women (CTRL) and 5 women affected by obesity (OBF), were compared in order to analyze the transcriptional differences present at tissue level.

RNA-sequencing analysis was performed with a cluster density of 174K/mm^2 and a cluster passing filter was 90.4%, indicating that the raw data obtained was in line with the expected values required for subsequent analyses. When filtering for transcripts with >20 reads, 30327 total variables were identified, 18674 of which were coding genes and 11653 of which were non-coding transcripts. Specific details on library quality are reported in our Data in Brief report (unpublished data, under review).

After RNA-Seq analysis, genes were analyzed according to their Fold Change (FC) and their False Discovery Rate (FDR). Genes showing $|\log2FC| \geq 1$ and an FDR ≤ 0.1 were considered as differentially expressed (DE RNAs). The differentially expressed genes were represented as heatmap (Figure 1A), and clustering analysis showed that OBF and CTRL clearly separated. Moreover, a volcano plot was built considering a total of 60,199 genes and it reports the dysregulation profile between OBF vs CTRL (Figure 1B). Specifically, a total of 171 differentially expressed RNAs (DE RNAs) were detected in SAT tissue from OBF versus CTRL (Table 1). Of these, 160 were coding genes (mRNAs; 127 up-regulated DE RNAs and 33 down-regulated DE RNAs) and 11 were non-coding genes (ncRNAs; 8 up-regulated DE RNAs and 3 down-regulated DE RNAs).

Table 1: Number of differentially expressed genes in the SAT of OBF vs. CTRL.

	OBF vs. CTRL		
	mRNAs	ncRNAs	Total
Up Regulated	127	8	135
Down Regulated	33	3	36
Total	**160**	**11**	**171**

The sub-type characterization of the ncRNAs is reported in Table 2 with a classification of these ncRNAs for their specific biotype. It is possible to observe how the most abundant category are Natural Antisense Transcripts (NATs), followed by long intergenic non-coding

RNAs (lincRNAs), both lncRNAs. As NATs and lincRNAs are the most abundant category of differentially expressed ncRNAs, we decided to focus on the role of lncRNAs for all further experiments and analyses.

Table 2: Biotype characterization of differentially expressed ncRNAs. TEC: To be Experimentally Confirmed; IG C pseudogene:inactivated immunoglobulin gene.

	ncRNAs		
	Up Regulated	Down Regulated	Total
NATs	3	1	4
lincRNAs	2	0	2
Processed pseudogene	0	1	1
TEC	0	1	1
Transcribed unprocessed pseudogene	1	0	1
IG_C_pseudogene	1	0	1
Unprocessed pseudogene	1	0	1
Total	**8**	**3**	**11**

A bibliographic analysis of previous literature was performed, in order to identify how many, amongst the 171 DE RNAs had been previously associated with obesity (Figure 1C). Almost half of the deregulated genes (47.37%) had never been associated with the obesity condition and moreover, most of the studies concerning the 90 obesity-associated genes were observational studies, correlating the genes to an obese phenotype (Figure 1C).

Role of the non-coding transcriptome in SAT from obese patients

The several non-coding DE RNAs that emerged as differentially expressed are reported as a volcano plot graph highlighting only the non-coding component (Figure 1D). Out of the 11 deregulated DE RNAs which emerge from transcriptional analysis of OBF vs. CTRL SAT, 6 belong to the lncRNAs category (Table 3). Most are uncharacterized genes, with unknown function, and interestingly three of them are NATs to coding genes (COL4A2, ITGB2, and RPS21). The common aliases for each will be used for now on: PELATON, COL4A2-AS2, CTEPHA1, RPS21-AS, ITGB2-AS1, ACER2-AS.

Table 3: List of lncRNAs DE in OBF vs CTRL SAT.

Gene_name	Log2FC	Aliases	Function
COL4A2-AS2	5.93		NAT to COL4A2, which pays a role in osteogenic differentiation and is differentially secreted in adipogenic differentiation.
SMIM25	2.74	GCRL1, LINC01272, PELATON	Nuclear expressed, monocyte- and macrophage-specific lncRNA, upregulated in unstable atherosclerotic plaque.
AL121832.2	2.36	RPS21-AS	NAT to RPS21, unknown function
ITGB2-AS1	2.23		NAT to ITGB2 and polymorphism in ITGB2 were associated with obesity.

LINC01094	1.74	CTEPHA1	Deregulated in post-menopausal osteoporosis, implicated in Chronic Thromboembolic Pulmonary Hypertension
AL158206.1	-1.07	ACER2-AS	NAT to ACER2, an alkaline ceramidase implicated in lipids metabolism.

A study of the coding/non-coding components interaction was done performing a WGCNA analysis, and the obtained network with a weighted correlation threshold of 0.1 are reported in Figure 1E. Specifically 8 ncRNAs emerge as part of the interactome and 6 of these are lncRNAs (reported in pink). RPS21-AS, CTEPHA1, and ITGB2-AS1 form three independent networks, whereas COL4A2-AS2, SMIM25 and ACER2-AS all take part in a main coding/non-coding correlation network (Figure 1E).

In silico characterization of 6 DE lncRNAs

We then decided to perform a specific computational dissection of each lncRNA in order to shed a preliminary light on their possible function in the adipose tissue and in obesity. An in detail dissection of all analyses performed is reported for COL4A2-AS2. COL4A2-AS2 is an antisense lncRNA to COL4A2, localized on the – strand of Chromosome 13 (Figure S1A). Its sequence was analyzed with the AnnoLnc2 database for further characterization. Repeat elements analysis through the RepeatMasker genomic datasets highlighted the presence of only one repeat element, MLT1C (of the LTR/ERVL-MaLR repeat class) (Table S3). We analyzed its sequence conservation with PhyloP and PhastCons scores, aimed at assessing base conservation amongst species (Figure S1B). PhyloP analysis highlights a tendency for fast evolution for exon sequences and a reduced conservation for promoter sequences. Conversely, PhastCons also indicates that the conservation score is not in the range of "conserved sequences", especially in primates, for both exon and promoter sequences. Derived Allele Frequency (DAF) score is around 0.35, suggesting that the gene is not under strong purifying selection. Moreover, we assessed its expression profile and found that COL4A2-AS2 is expressed mainly in the adipose tissue, blood vessels and nerves (Figure 2A). Analysis of localization motifs indicated the presence of nuclear-localization domains, although analysis of localization from nuclear and cytosolic RNA-seq samples of 10 cell lines from ENCODE indicated a cytoplasmic localization for the lncRNA (Figure S1C, Table S4). The secondary structure prediction could be useful in the identification of miRNA (Figure S1D and Table S5) and protein binding sites (identified via CLIP-Seq, Figure S1E and Table S6), which could modulate the lncRNAs expression and mechanism of action. AnnoLnc2 through GTRD database allowed to highlight peak clusters of transcription factors (TFs) in adipocytes, and these specifically are CTCF, PPARG and RELA (Table S7). We also cross-referenced all the genes which emerged as positively correlated with COL4A2-AS2 with the DE RNAs from our RNA-seq analysis and found that there were no match in this case (Figure S1F). Lastly, we investigated the biological processes positively correlated with this lncRNAs and we report the top 20 significant pathways in Figure 2B. Remarkably the most significant pathway pertained +ve regulation of fat cell differentiation, and other relevant processes include "regulation of cellular response to insulin stimulus" and "regulation of fat cell differentiation".

RPS21-AS (AL121832.2) is also localized on Chromosome 20, on the – strand, opposite to RPS21, a ribosomal protein (Figure S2A). It presents a LINE repeat element (Table S3), its exon appears fast evolving and under strong purifying selection, differently from the promoter (Figure S2B), and it has a ubiquitary expression (mainly in the testis, Figure 2C). It presents a nuclear motif (Table S4) but localizes in the cytosol in 7/10 studied cell lines (Figure S2C), it presents binding sites for 19 miRNAs (Figure S2D and Table S5), has 87 interactions with proteins (Figure S2E and Table S6) and it is modulated by KLF11, CTCF and PPARG in adipocytes (Table S7). It has 3883 positively correlated genes, none present amongst our DE RNAs, and it correlates with response to stimulus and sexual reproduction (male gametes, Figure 2D).

PELATON is localized on the + strand of Chromosome 20 (Figure S3A), it presents repeat elements of the SINE and LINE class (Table S3) and its sequence does not appear to be highly conserved, although its promoter is under strong purifying selection (Figure S3B). It presents nuclear localization binding motifs (Table S4) but it localizes in the cytoplasm in HeLa cells (Figure S3C) and it is mainly expressed in the blood, lung, spleen and adipose tissue (Figure 3A). It is predicted to interact with 70 miRNA (Figure S3D and Table S5), it is bound by FUS (Figure S3E and Table S6) and it is regulated by 5 TFs in adipocytes (PPARG, CTCF, RELA and EP300, Table S7). Amongst the 639 positively correlated genes, 15 are DE RNAs from our datasets, and for two of them, DOK3 and TYROBP, a *trans* regulation has been found (LncEXPdb, Figure 3B). Moreover, it positively correlates with immunogenic processes (Figure 3C).

ITGB2-AS1 localizes on the + strand on Chromosome 21, antisense to ITGB2 (Figure S4A). It presents a LINE and a single repeat (Table S3), it does not appear to be strongly conserved nor under strong purifying selection (Figure S4B) and no data is currently present on its localization, though it is enriched mainly in the blood, lung, and spleen (Figure 3D). It presents 78 miRNA (Figure S4C and Table S5) binding sites, it is also bound by FUS (Figure S4D, Table S6) and presents binding sites in adipocytes for CEBPA, CTCF, LMNA, MBD4, PPARG and RELA (Table S7). It positively correlates with 421 genes, amongst them 7 are DE RNAs, and specifically with EVI2B and CTSS it was found to interact in *trans* (LncEXPdb, Figure 3E) and it also appears implicated in immunogenic processes (Figure 3F).

ACER2-AS (AL158206.1) localizes on the + strand of Chromosome 9, antisense to ACER2 (Figure S5A), it presents two single repeats (Table S3), it appears to be more conserved than fast evolving (especially its exon, Figure S5B), it localizes in the cytosol in 6/10 analyzed cell lines but presents nuclear retention motives (Figure S5C and Table S4) and it is mainly enriched in the adipose tissue (Figure 4A). It has binding sites for 60 miRNAs (Figure S5D and Table S5), 69 proteins (Figure S5E and Table S6) and PPARG in SAT (Table S7). Out of the 14 positively correlated genes there are ACER2-AS itself and ACER2, both DE RNAs (Figure 4B), and the RNA appears implicated in Acyl-CoA biosynthetic processes (Figure 4C).

The last DE ncRNA is CTEPHA1, localized on the + strand of Chromosome 4 (Figure S6A), with 7 repeat elements (Table S3), it appears to be rather conserved (Figure S6B), with a cytoplasmic localization (Figure S6C, although a nuclear motif, Table S4) and a predominant

expression in the blood and vagina (Figure 4D). The binding sites for miRNAs, proteins and TFs in adipocytes are respectively 145 (Figure S6D and Table S5), 1 (Figure S6E and Table S6) and 10 (Table S7, with CEBPA amongst them). It is positively correlated with 7 DE RNAs (Figure 4E) and it is involved in immune system processes (Figure 4F).

LncRNAs present time-point specific deregulation during adipogenic differentiation

As our RNA-seq highlighted that these lncRNAs have been found to be deregulated in SAT of obese patients, in vitro differentiation experiments were performed to investigate their role in adipogenesis, both in obesity-affected patients and in healthy subjects. We firstly analyzed the expression of the 6 lncRNAs in SAT mesenchymal stem cells from obese patients, along with the sense genes RPS21 and COL4A2, in order to assess whether dysfunctions observed at whole tissue level were also recapitulated during adipogenic processes in obesity affected patients. Cells were differentiated for 14 days under standard adipogenic differentiation protocol and all of the lncRNAs present changes in expression along different phases of differentiation (Figure 5A, Figure S7A). Interestingly, in the case of CTEPHA1, ITGB2-AS1 and COL4A2-AS2, the expression seems to initially decrease in a divergent manner to that of obese patients-derived hADSCs and this indicates the genes could act differently at whole tissue level as opposed to cellular differentiation. The other genes present an increase during adipogenic differentiation. The genes expression was also analyzed during the differentiation of hADSCs obtained from the lipoaspirate of a healthy subject used as control (CTRL), in order to assess whether these lncRNAs could also play a role in adipogenesis of healthy subjects (Figure 5B, Figure S7B). Also, in this case the expression of the lncRNAs and sense genes changes at the different phasis of the adipogenesis process, and they all seem to present a peak at day 7, with the highest significance for PELATON, RPS21-AS, CTEPHA1, COL4A2 and RPS21 (Figure 5B, Figure S7C). Interestingly, in the case of CTEPHA1, ITGB2-AS1, PELATON, COL4A2-AS2 and COL4A2, the expression seems to peak at day 7, with a subsequent decrease. On the contrary, for ACER2-AS, RPS21-AS and RPS21, the increase seems to be constant and maintained up to day 14 (Figure 5B, Figure S7D). Moreover, the pattern of sense/antisense genes is not necessarily concordant, but this is in line with reports highlighting a function for antisense gene in both positive regulation and inhibition of sense genes expression (39).

LncRNAs can be selectively modulated by adipogenesis-related transcription factors

As there is a time-point specific alteration of the lncRNAs expression we investigated whether this could be due to adipogenesis-TFs regulation, as these lncRNAs present TFs binding sites in their promoter sequence (Table S7). We thus decided to modulate the expression of C/EBPβ, C/EBPδ, C/EBPα and PPARγ, as these are known TFs regulating adipogenesis. To do so, we silenced the expression of the C/EBPs via RNA interference (Figures 6A-C, S8A-C). Specifically, we found that C/EBPβ significantly influenced RPS21-AS, ITGB2-AS1, ACER2-AS and CTEPHA1 (Figure 6A), whereas PELATON, ITGB2-AS1, ACER2-AS and CTEPHA1 were significantly reduced when the expression of C/EBPδ was decreased (Figure 6B) and lastly PELATON, ITGB2-AS1 and CTEPHA1 were decreased by C/EBPα inhibition (Figure 6C). As PPARγ is known to be adipogenesis' master regulator (40, 41), its influence on the investigated lncRNAs and respective sense genes was analyzed. To

do so, its activity was induced with the pharmacological activator troglitazone in undifferentiated conditions (34), whilst we inhibited it with the inhibitor T0070907 administered during adipogenic differentiation (Figure 6D, Figure S8C). COL4A2-AS2, PELATON and CTEPHA1 were induced by PPARγ's activation, whilst ITGB2-AS1 appears to be inhibited by it (conversely with its trend during differentiation). Moreover, all the lncRNAs were induced during differentiation except for but ITGB2-AS1, which was decreased. The treatment with the PPARγ inhibitor did not appear to influence their expression (Figure 6D).

The lncRNA CTEPHA1 could have a role in adipogenesis through the modulation of C/EBPα expression

To further understand the complex network of involvement for lncRNAs in adipogenesis we decided to modulate the expression of CTEPHA1 via RNA interference and subsequently assess the expression levels of adipogenesis-related genes (C/EBPβ, C/EBPδ, C/EBPα and PPARγ). We found a successful inhibition of CTEPHA1, and we report that this does not appear to influence the early adipogenesis regulators C/EBPβ and C/EBPδ (Figure 6E). On the contrary, its inhibition appears to be correlated with the reduced expression of C/EBPα and PPARγ, suggesting that CTEPHA1 could influence later stages of adipogenesis. Indeed, the most significant down-regulation is observed for C/EBPα, and this could be the TFs on which CTEPHA1 acts the most, in a positive feedback loop even as C/EBPα's downregulation also inhibits CTEPHA1 (Figure 6C, Figure 6E).

Role of the coding transcriptome in SAT from obese patients

We subsequently decided to perform a comprehensive *in silico* dissection of the deregulated dataset, and in order to ensure a higher significance for the in silico prediction, we selected those genes with an FDR ≤ 0.05. We thus obtained a total of 83 genes, of which 3 were non coding genes (Table 4, Supplementary Table 8)

Table 4: Number of differentially expressed genes with FDR ≤ 0.05 in SAT of OBF vs. CTRL.

	OBF vs. CTRL		
	mRNAs	ncRNAs	Total
Up Regulated	57	2	59
Down Regulated	23	1	24
Total	**80**	**3**	**83**

We then decided to analyze the top 20 DE RNAs based on their FC (Table 5). These include lncRNAs (COL4A2-AS2), along with genes implicated in the immune system, tissue re-modelling and biology of striatal muscle.

Table 5: FC of Top 20 DE RNAs. Protein function description was obtained from the STRING database.

Gene Name	FC	p value	Gene Function

COL4A2-AS2	5.93	0.00014	Unknown.
MMP7	5.72	0.000018	Matrilysin; Degrades casein, gelatins of types I, III, IV, and V, and fibronectin.
DES	-5.67	0.00000026	Desmin; Muscle-specific type III intermediate filament essential for proper muscular structure and function.
ADAMDEC1	5.26	0.000018	Important role in the control of the immune response.
TREM2	5.20	0.0000011	Triggering receptor expressed on myeloid cells 2; Forms a receptor signaling complex with TYROBP.
SPP1	5.09	0.0000071	Osteopontin; Binds tightly to hydroxyapatite. Forms an integral part of the mineralized matrix. Important to cell-matrix interaction.
TM4SF19	4.98	0.0000034	Transmembrane 4 L six family member 19; Belongs to the L6 tetraspanin family.
MMP8	4.70	0.000028	Neutrophil collagenase; Can degrade fibrillar type I, II, and III collagens; Belongs to the peptidase M10A family.
DCSTAMP	4.63	0.000025	Dendritic cell-specific transmembrane protein; Cell surface receptor, roles in cellular fusion, cell differentiation, bone and immune homeostasis. Role in TNFSF11-mediated osteoclastogenesis.
PDE6G	4.32	0.000016	Retinal rod rhodopsin-sensitive cGMP 3',5'-cyclic phosphodiesterase subunit gamma; Implicated in transmission of the visual signal.
TM4SF19-TCTEX1D2	4.12	0.00011	Unknown.
SDS	4.10	0.000015	L-serine dehydratase/L-threonine deaminase; Serine dehydratase.
TNNI2	3.96	0.00021	Troponin I, fast skeletal muscle; Inhibitory subunit of troponin, the thin filament regulatory complex which confers calcium-sensitivity to striated muscle actomyosin ATPase activity.
CD300LB	3.77	0.000038	CMRF35-like molecule 7; Acts as an activating immune receptor through its interaction with ITAM-bearing adapter TYROBP, and also independently by recruitment of GRB2.
APOC1	3.75	0.000075	Apolipoprotein C-I; Inhibitor of lipoprotein binding to the low-density lipoprotein (LDL) receptor, LDL receptor-related protein, and very low-density lipoprotein (VLDL) receptor.
CD52	3.73	0.000013	CAMPATH-1 antigen; May play a role in carrying and orienting carbohydrate, as well as having a more specific role.
ACTG2	-4.27	0.011	Actin, gamma-enteric smooth muscle; Actins are highly conserved proteins that are involved in various types of cell motility and are ubiquitously expressed in all eukaryotic cells.
ANLN	4.44	0.0076	Anillin; Required for cytokinesis. Essential for the structural integrity of the cleavage furrow and for completion of cleavage furrow ingression. Plays a role in bleb assembly during metaphase and anaphase of mitosis.
ACP5	4.50	0.00664	Tartrate-resistant acid phosphatase type 5; Involved in osteopontin/bone sialoprotein dephosphorylation. Belongs to the metallophosphoesterase superfamily.
SDC1	3.94	0.029	Syndecan-1; Cell surface proteoglycan that bears both heparan sulfate and

			chondroitin sulfate and that links the cytoskeleton to the interstitial matrix. Regulates exosome biogenesis in concert with SDCBP and PDCD6IP

The subcellular localization of a protein can help infer its possible function, and moreover a global look at the localization of the DE RNAs can help identify the compartments most affected by the dysregulation. When looking at the subcellular localization of DE RNAs, a high number of organelles emerge, suggesting that the cells of the SAT present with ubiquitary perturbations, in the nucleus as well as the cytoplasm, the mitochondria, and the cytoskeleton indicating a profound alteration in all cellular functions (Figure 7A).

GO terms enrichment and pathways analysis

We then performed a GSEA for GO and pathways analysis, in order to consider the whole perturbation happening in SAT (Figure 7B-F). The Biological Processes analysis highlighted positive enrichment involved in immune system response (B cell activation and antigen receptor signaling pathway), whilst there is a negative enrichment for metabolic processes (ATP and amino acid) (Figure 7B). Similarly, Molecular Function also highlighted a positive enrichment in immune system process and channel activity (Figure 7C). Interestingly, a negative enrichment is present for gene expression modulation, with processes implicated in transcription and translation (Figure 7C). Concordantly, Cellular Component analysis highlighted a positive enrichment in immune-related complexes whilst a negative enrichment in nuclear and mitochondrial components (Figure 7D). KEGG pathway analysis highlighted also a positive enrichment in genes associated with autoimmune diseases (e.g. autoimmune thyroid disease, systemic lupus erythematosus and asthma), whilst there is a negative enrichment in metabolic pathways (Figure 7E). WikiPathways analysis also shows the same results (Figure 7F).

Obesity association with co-occurring diseases

As obesity is known to increase the risk of co-morbidities development, we aimed to identify which deregulated genes are specifically responsible for this phenomenon. Via the DisGENET database we reported the known interaction of the DE RNAs with an FDR ≤ 0.05 with diseases of Nutritional and Metabolic Diseases and the Immune System, obtained from curated databases (Figure 8A, 8B). When we analyzed all known interactions between the DE RNAs and nutritional and metabolic diseases as obtained from curated databases we found canonical metabolic diseases such as diabetes and celiac disease, along with diseases of the central nervous system diseases with a metabolic component, such as central nervous system inborn metabolic diseases, brain metabolic diseases, amyotrophic lateral sclerosis, semantic dementia etc. (Figure 8A). For the Immune System, numerous diseases were implicated including multiple types of diabetes, known complication of obesity, but also autoimmune diseases such as Lupus Erythematosus Systemic, Rheumatoid Arthritis, Immunologic Deficiency Syndromes, Multiple Sclerosis, defects in the leucocyte adhesion process, dermal diseases etc. (Figure 8B). When expanding the search to all known databases, 27 genes were found to be significantly associated with obesity (Figure 8C). As negative controls, we run the gene-set against un-related disease classes such as “infections” and “animal diseases”, which

returned no terms. Moreover, we run a search of 83 randomly selected terms (Supplementary Table 9) for the same databases, and the correlations present are reported for nutritional and metabolic diseases (Supplementary Figure 9A), immune system diseases (Supplementary Figure 9B) and obesity in all known databases (Supplementary Figure 9C). In these cases, only two genes per network emerged, highlighting that the connection reported in Figure 8 is specific of our dataset.

Discussion

Obesity is a very severe condition which can lead to an increase in associated morbidities for many chronic diseases such as T2D, hypertension, coronary artery disease, dyslipidemia, stroke, osteoarthritis, certain forms of cancer (1-3), and ultimately result in an increased mortality rate (1). To this day, it is not possible to have conclusive data on what is the relative contribution of either genetic or the environment on obesity onset. Indeed, behavior and genes are different levels of the same causal framework, and epigenetics through RNA biology has been suggested to play a central role in elucidating new targetable pathways. We previously highlighted the presence of different transcriptional profiles in obesity-affected men and women, highlighting gender-specific differences in transcription profiles, and we also performed a characterization of the oncogenic susceptibility present in SAT tissues of normal weight subjects, obesity-affected women, obesity and type 2 diabetes-affected women and obesity-affected men (4, 22). In this study we have characterized the differences in the transcriptional profiles of SAT from normal weight and obesity-affected women, with a particular interest on the role of long non-coding RNAs. Remarkably, amongst the 171 DE RNAs identified here, 81 had never been correlated to obesity before and could thus be of great relevance for future characterization in the obesogenic context. The non-coding transcriptome was found to be significantly implicated, and we focused our further characterization on lncRNAs as this class of molecules are showing to have a relevant function in the pathogenesis of numerous metabolic diseases, including obesity (16, 42-45). The identification of co-interaction networks allowed us to identify 6 lncRNAs which could influence numerous coding genes found altered via RNA-seq, thus suggesting a potential their involvement in the altered signaling pathways present in obesity (22, 46, 47). The 6 lncRNAs identified were COL4A2-AS2, RPS21-AS, PELATON, ITGB2-AS1, ACER2-AS and CTEPHA1, and for each of them we performed a further characterization both *in silico* and *in vitro* differentiation of hADSCs. We report that these are expressed in the adipose tissue, present binding sites for adipogenesis-related TFs and are also implicated in adipogenesis related biological processes such as regulation of fat cell differentiation (COL4A2-AS2), immune response (PELATON, ITGB2-AS1 and CTEPHA1) and metabolic processes (ACER2-AS).

When analyzing their deregulation in different phases of adipogenic differentiation process, they all present different expression levels during adipogenesis in mesenchymal stem cells obtained from both obese and healthy subjects. Although these are different biological scenarios compared to the whole tissue analysis, performed through RNA-seq, these in vitro models allow to question whether the dysfunctions observed in SAT could be recapitulated in early stages of tissue development, such as those represented by adipogenesis. Interestingly,

whilst the RNA-seq characterized coding and non-coding genes implicated in obese-derived SAT, we found an implication for the investigated lncRNAs also in adipogenesis processes of healthy patients, suggesting a role for these molecules in the regulation of the process.

We identified, for the first time, a modulation of the lncRNAs by C/EBPβ, C/EBPδ and C/EBPα, along with a role for PPARγ in modulating these genes. Even if the genes do not present binding sites for all these transcription factors, there could be a trans modulation of the lncRNAs expression, as these are primary regulators of a network that is indeed complex and rich in other key players (48, 49). Specifically, the lncRNAs expression appears to be impacted mostly by C/EBPs dysregulation in expression. Moreover, we investigated whether the lncRNAs, focusing on CTEPHA1, could also influence the TFs expression, and found that CTEPHA1 inhibition also led to a decreased expression in late adipogenesis modulators, with a specific relevance for C/EBPα. Indeed, adipogenesis is a complex network governed by a multitude of regulators, and lncRNAs could be important players in it (48-50). These molecules present modes of action both in cis, in proximity to their gene locus, and in trans, governing the action of genes which do not necessarily relate to their chromosomal localization (15, 16, 21, 45, 51).

We also performed a dissection of localization and pathways dysregulation from coding genes, and found a significant implication for the immune system, to be expected as the SAT from obese patients presents a high degree of fibrosis, along with tissue remodeling and, interestingly, the biology of the striatal muscle. Indeed, obesity can cause a decline in contractile function of skeletal muscle, thereby reducing mobility and leading to the development of even more obesity-associated health risks (52). KEGG and WikiPathways analyses highlighted also a positive enrichment in genes associated with autoimmune diseases (e.g. autoimmune thyroid disease, systemic lupus erythematosus and asthma), whilst there is a negative enrichment in metabolic pathways. The gene expression signature is also correlated with multiple diseases insurgence, such as immune system diseases and nutritional and metabolic system diseases. The research presented here was possibly limited by the small sample-size and further technical validation in different adipose depots as well as confirmation data in wider cohorts with related follow-up studies are certainly needed.

Overall, our findings are a thorough characterization of transcriptional dysregulation present in subcutaneous adipose tissue of obesity-affected patients. Our results highlight a clear implication for 6 never described lncRNAs in adipogenesis network, adding them as new players and regulators to the adipocyte biology, with implications for human obesity. Indeed, these molecules could prove to be biomarkers relevant for early intervention, or useful tools in the development of future precision medicine strategies.

References

1. WHO. Obesity and Overweight World Health Organization2020 [Available from: https://www.who.int/news-room/fact-sheets/detail/obesity-and-overweight.
2. Haslam D, Sattar N, Lean M. ABC of obesity. Obesity--time to wake up. BMJ. 2006;333(7569):640-2.
3. Lawrence VJ, Kopelman PG. Medical consequences of obesity. Clin Dermatol. 2004;22(4):296-302.
4. Rey F, Messa L, Pandini C, Launi R, Barzaghini B, Micheletto G, et al. Transcriptome Analysis of Subcutaneous Adipose Tissue from Severely Obese Patients Highlights Deregulation Profiles in Coding and Non-Coding Oncogenes. Int J Mol Sci. 2021;22(4).
5. Wyatt HR. Update on treatment strategies for obesity. J Clin Endocrinol Metab. 2013;98(4):1299-306.
6. Singh RK, Kumar P, Mahalingam K. Molecular genetics of human obesity: A comprehensive review. C R Biol. 2017;340(2):87-108.
7. Stöger R. Epigenetics and obesity. Pharmacogenomics. 2008;9(12):1851-60.
8. Loh M, Zhou L, Ng HK, Chambers JC. Epigenetic disturbances in obesity and diabetes: Epidemiological and functional insights. Molecular Metabolism. 2019;27:S33-S41.
9. Allum F, Grundberg E. Capturing functional epigenomes for insight into metabolic diseases. Molecular Metabolism. 2020;38:100936.
10. St Laurent G, Wahlestedt C, Kapranov P. The Landscape of long noncoding RNA classification. Trends Genet. 2015;31(5):239-51.
11. Boden G, Duan X, Homko C, Molina EJ, Song W, Perez O, et al. Increase in endoplasmic reticulum stress-related proteins and genes in adipose tissue of obese, insulin-resistant individuals. Diabetes. 2008;57(9):2438-44.
12. Arner P, Kulyté A. MicroRNA regulatory networks in human adipose tissue and obesity. Nat Rev Endocrinol. 2015;11(5):276-88.
13. Chen J, Cui X, Shi C, Chen L, Yang L, Pang L, et al. Differential lncRNA expression profiles in brown and white adipose tissues. Mol Genet Genomics. 2015;290(2):699-707.
14. Sun L, Goff LA, Trapnell C, Alexander R, Lo KA, Hacisuleyman E, et al. Long noncoding RNAs regulate adipogenesis. Proc Natl Acad Sci U S A. 2013;110(9):3387-92.
15. Gao H, Kerr A, Jiao H, Hon CC, Rydén M, Dahlman I, et al. Long Non-Coding RNAs Associated with Metabolic Traits in Human White Adipose Tissue. EBioMedicine. 2018;30:248-60.
16. Rey F, Urrata V, Gilardini L, Bertoli S, Calcaterra V, Zuccotti GV, et al. Role of long non-coding RNAs in adipogenesis: State of the art and implications in obesity and obesity-associated diseases. Obes Rev. 2021.
17. Alvarez-Dominguez JR, Bai Z, Xu D, Yuan B, Lo KA, Yoon MJ, et al. De Novo Reconstruction of Adipose Tissue Transcriptomes Reveals Long Non-coding RNA Regulators of Brown Adipocyte Development. Cell Metab. 2015;21(5):764-76.
18. Salem ESB, Vonberg AD, Borra VJ, Gill RK, Nakamura T. RNAs and RNA-Binding Proteins in Immuno-Metabolic Homeostasis and Diseases. Front Cardiovasc Med. 2019;6:106.
19. Landrier JF, Derghal A, Mounien L. MicroRNAs in Obesity and Related Metabolic Disorders. Cells. 2019;8(8).
20. Arcinas C, Tan W, Fang W, Desai TP, Teh DCS, Degirmenci U, et al. Adipose circular RNAs exhibit dynamic regulation in obesity and functional role in adipogenesis. Nature Metabolism. 2019;1(7):688-703.
21. Rey F, Zuccotti GV, Carelli S. Long non-coding RNAs in metabolic diseases: from bench to bedside. Trends Endocrinol Metab. 2021.

22. Rey F, Messa L, Pandini C, Maghraby E, Barzaghini B, Garofalo M, et al. RNA-seq Characterization of Sex-Differences in Adipose Tissue of Obesity Affected Patients: Computational Analysis of Differentially Expressed Coding and Non-Coding RNAs. J Pers Med. 2021;11(5).
23. Gerhardt CC, Romero IA, Cancello R, Camoin L, Strosberg AD. Chemokines control fat accumulation and leptin secretion by cultured human adipocytes. Mol Cell Endocrinol. 2001;175(1-2):81-92.
24. Yu G, Wang LG, Han Y, He QY. clusterProfiler: an R package for comparing biological themes among gene clusters. OMICS. 2012;16(5):284-7.
25. Zhu A, Ibrahim JG, Love MI. Heavy-tailed prior distributions for sequence count data: removing the noise and preserving large differences. Bioinformatics. 2019;35(12):2084-92.
26. Pratt D, Chen J, Welker D, Rivas R, Pillich R, Rynkov V, et al. NDEx, the Network Data Exchange. Cell Syst. 2015;1(4):302-5.
27. Shannon P, Markiel A, Ozier O, Baliga NS, Wang JT, Ramage D, et al. Cytoscape: a software environment for integrated models of biomolecular interaction networks. Genome Res. 2003;13(11):2498-504.
28. Li J, Zhou D, Qiu W, Shi Y, Yang J-J, Chen S, et al. Application of Weighted Gene Co-expression Network Analysis for Data from Paired Design. Scientific Reports. 2018;8(1):622.
29. Ke L, Yang DC, Wang Y, Ding Y, Gao G. AnnoLnc2: the one-stop portal to systematically annotate novel lncRNAs for human and mouse. Nucleic Acids Res. 2020;48(W1):W230-W8.
30. Li Z, Liu L, Jiang S, Li Q, Feng C, Du Q, et al. LncExpDB: an expression database of human long non-coding RNAs. Nucleic Acids Res. 2021;49(D1):D962-D8.
31. Carelli S, Messaggio F, Canazza A, Hebda DM, Caremoli F, Latorre E, et al. Characteristics and Properties of Mesenchymal Stem Cells Derived From Microfragmented Adipose Tissue. Cell Transplant. 2015;24(7):1233-52.
32. Carelli S, Colli M, Vinci V, Caviggioli F, Klinger M, Gorio A. Mechanical Activation of Adipose Tissue and Derived Mesenchymal Stem Cells: Novel Anti-Inflammatory Properties. Int J Mol Sci. 2018;19(1).
33. Kawaji A, Ohnaka Y, Osada S, Nishizuka M, Imagawa M. Gelsolin, an actin regulatory protein, is required for differentiation of mouse 3T3-L1 cells into adipocytes. Biol Pharm Bull. 2010;33(5):773-9.
34. Rey F, Lesma E, Massihnia D, Ciusani E, Nava S, Vasco C, et al. Adipose-Derived Stem Cells from Fat Tissue of Breast Cancer Microenvironment Present Altered Adipogenic Differentiation Capabilities. Stem Cells Int. 2019;2019:1480314.
35. Galateanu B, Dinescu S, Cimpean A, Dinischiotu A, Costache M. Modulation of adipogenic conditions for prospective use of hADSCs in adipose tissue engineering. Int J Mol Sci. 2012;13(12):15881-900.
36. Hausman GJ, Dodson MV, Ajuwon K, Azain M, Barnes KM, Guan LL, et al. Board-invited review: the biology and regulation of preadipocytes and adipocytes in meat animals. J Anim Sci. 2009;87(4):1218-46.
37. Lee G, Elwood F, McNally J, Weiszmann J, Lindstrom M, Amaral K, et al. T0070907, a selective ligand for peroxisome proliferator-activated receptor gamma, functions as an antagonist of biochemical and cellular activities. J Biol Chem. 2002;277(22):19649-57.
38. Livak KJ, Schmittgen TD. Analysis of relative gene expression data using real-time quantitative PCR and the 2(-Delta Delta C(T)) Method. Methods. 2001;25(4):402-8.
39. Zhou M, Guo X, Wang M, Qin R. The patterns of antisense long non-coding RNAs regulating corresponding sense genes in human cancers. J Cancer. 2021;12(5):1499-506.

40. Zhuang H, Zhang X, Zhu C, Tang X, Yu F, Shang GW, et al. Molecular Mechanisms of PPAR-γ Governing MSC Osteogenic and Adipogenic Differentiation. Curr Stem Cell Res Ther. 2016;11(3):255-64.
41. Lefterova MI, Haakonsson AK, Lazar MA, Mandrup S. PPARγ and the global map of adipogenesis and beyond. Trends Endocrinol Metab. 2014;25(6):293-302.
42. Squillaro T, Peluso G, Galderisi U, Di Bernardo G. Long non-coding RNAs in regulation of adipogenesis and adipose tissue function. Elife. 2020;9.
43. Wijesinghe SN, Nicholson T, Tsintzas K, Jones SW. Involvements of long noncoding RNAs in obesity-associated inflammatory diseases. Obes Rev. 2020.
44. Babapoor-Farrokhran S, Gill D, Rasekhi RT. The role of long noncoding RNAs in atrial fibrillation. Heart Rhythm. 2020;17(6):1043-9.
45. Ji E, Kim C, Kim W, Lee EK. Role of long non-coding RNAs in metabolic control. Biochim Biophys Acta Gene Regul Mech. 2020;1863(4):194348.
46. Tait S, Baldassarre A, Masotti A, Calura E, Martini P, Varì R, et al. Integrated Transcriptome Analysis of Human Visceral Adipocytes Unravels Dysregulated microRNA-Long Non-coding RNA-mRNA Networks in Obesity and Colorectal Cancer. Front Oncol. 2020;10:1089.
47. Chen Y, Li K, Zhang X, Chen J, Li M, Liu L. The novel long noncoding RNA lncRNA-Adi regulates adipogenesis. Stem Cells Transl Med. 2020.
48. Lee JE, Schmidt H, Lai B, Ge K. Transcriptional and Epigenomic Regulation of Adipogenesis. Mol Cell Biol. 2019;39(11).
49. Kuri-Harcuch W, Velez-delValle C, Vazquez-Sandoval A, Hernández-Mosqueira C, Fernandez-Sanchez V. A cellular perspective of adipogenesis transcriptional regulation. J Cell Physiol. 2019;234(2):1111-29.
50. Ghaben AL, Scherer PE. Adipogenesis and metabolic health. Nature Reviews Molecular Cell Biology. 2019;20(4):242-58.
51. Latorre J, Fernández-Real JM. LncRNAs in Adipose Tissue from Obese and Insulin-Resistant Subjects: New Targets for Therapy? EBioMedicine. 2018;30:10-1.
52. Tallis J, James RS, Seebacher F. The effects of obesity on skeletal muscle contractile function. J Exp Biol. 2018;221(Pt 13).

Figure Legends

Figure 1. Global transcriptional deregulation in coding and non-coding genes is present in SAT from OBF and CTRL. (A) Expression profiles of differently expressed genes in OBF versus CTRL reported as a Heatmap. **(B)** Volcano plot showing deregulated genes between OBF and CTRL. On the x axis is reported the log_2FC whereas on the y axis is reported the P value in logarithmic scale. **(C)** pie chart of genes previously associated with obesity. **(D)** Volcano plot showing deregulated non-coding genes between OBF and CTRL. On the x axis is reported the log_2FC whereas on the y axis is reported the P value in logarithmic scale. **(E)** WGCNA of OBF vs. CTRL highlighting lncRNAs. The correlation threshold was set to 0.1 and the lncRNAs are reported in pink, whilst other ncRNAs are reported in green. The thicker edges refer to the first-degree interactions of non-coding DE RNAs.

Figure 2. In silico dissection of COL4A2-AS2 and RPS21-AS.
(A) Tissue expression data of COL4A2-AS2 as obtained with AnnoLnc2 database **(B)** BP of the pathways positively correlated with COL4A2-AS2 in normal tissue obtained with the AnnoLnc2 database and reproduced as bar plot graph. On the Y axis the pathway name, on the x axis the -

log(p.value) of the pathway. **(C)** Tissue expression data of RPS21-AS as obtained with AnnoLnc2 database **(D)** BP of the pathways positively correlated with COL4A2-AS2 in normal tissue obtained with the AnnoLnc2 database and reproduced as bar plot graph. On the Y axis the pathway name, on the x axis the -log(p.value) of the pathway.

Figure 3. In silico dissection of PELATON and ITGB2-AS1.
(A) Tissue expression data of PELATON as obtained with AnnoLnc2 database **(B)** Network of genes positively correlated with PELATON present in the AnnoLnc2 database cross-referenced with the DE RNAs present in this dataset. The LncEXPdb was used to identify potential correlation in cis and trans, which when present are reported on the graph. The network was built with Cytoscape and the color scale refers to the genes expression in terms of Log2FC **(C)** BP of the pathways positively correlated with PELATON in normal tissue obtained with the AnnoLnc2 database and reproduced as bar plot graph. On the Y axis the pathway name, on the x axis the -log(p.value) of the pathway. **(D)** Tissue expression data of ITGB2-AS1 as obtained with AnnoLnc2 database **(B)** Network of genes positively correlated with ITGB2-AS1 present in the AnnoLnc2 database cross-referenced with the DE RNAs present in this dataset. The LncEXPdb was used to identify potential correlation in cis and trans, which when present are reported on the graph. The network was built with Cytoscape and the color scale refers to the genes expression in terms of Log2FC **(D)** BP of the pathways positively correlated with ITGB2-AS1 in normal tissue obtained with the AnnoLnc2 database and reproduced as bar plot graph. On the Y axis the pathway name, on the x axis the -log(p.value) of the pathway.

Figure 4. In silico dissection of ACER2-AS and CTEPHA1.
(A) Tissue expression data of ACER2-AS as obtained with AnnoLnc2 database **(B)** Network of genes positively correlated with ACER2-AS present in the AnnoLnc2 database cross-referenced with the DE RNAs present in this dataset. The LncEXPdb was used to identify potential correlation in cis and trans, which when present are reported on the graph. The network was built with Cytoscape and the color scale refers to the genes expression in terms of Log2FC **(C)** BP of the pathways positively correlated with ACER2-AS in normal tissue obtained with the AnnoLnc2 database and reproduced as bar plot graph. On the Y axis the pathway name, on the x axis the -log(p.value) of the pathway. **(D)** Tissue expression data of CTEPHA1 as obtained with AnnoLnc2 database **(B)** Network of genes positively correlated with CTEPHA1 present in the AnnoLnc2 database cross-referenced with the DE RNAs present in this dataset. The LncEXPdb was used to identify potential correlation in cis and trans, which when present are reported on the graph. The network was built with Cytoscape and the color scale refers to the genes expression in terms of Log2FC **(D)** BP of the pathways positively correlated with CTEPHA1 in normal tissue obtained with the AnnoLnc2 database and reproduced as bar plot graph. On the Y axis the pathway name, on the x axis the -log(p.value) of the pathway.

Figure 5. LncRNAs expression during adipogenic differentiation of ADSCs of normal weight and obese subjects. (A) Differential expression of lncRNAs in adipocytes obtained from SAT tissue from obese patients was verified by Real Time PCR. 18S was used as housekeeping gene. Data are expressed as mean of 2 samples ± SEM (n = 2), * $p < 0.05$ vs. SAT Day 0. **(B)** Differential expression of lncRNAs in lipoaspirate of a CTRL subject was verified by Real Time PCR. GAPDH

was used as housekeeping gene. Data are expressed as mean of 3 experiments each performed in duplicates ± SEM (n = 6), * p < 0.05, **p<0.01, ***p<0.001 vs. Day 0.

Figure 6. Adipogenic transcription factors modulation of lncRNAs and sense genes. Differential expression of lncRNAs in hADSCs silenced for C/EBPβ **(B)**, C/EBPδ **(C)**, C/EBPα **(D)** versus control (siNEG) was verified by Real Time PCR. 18S was used as housekeeping gene. Data are expressed as mean of 3 experiments each performed in duplicates ± SEM (n = 6), * p < 0.05, **p<0.01, ***p<0.001 vs siNEG. **(E)** Expression of lncRNAs in hADSCs from healthy patients treated in undifferentiated conditions (UNDIFF), differentiated for 7 days in standard adipogenic medium (DIFF), in undifferentiated condition supplemented with Troglitazone (UNDIFF+TRO) and differentiated for 7 days in standard adipogenic medium supplemented with the PPARγ inhibitor T0070907 (DIFF + αPPARγ). Expression was verified by Real Time PCR and 18S was used as housekeeping gene. Data are expressed as mean of 3 experiments each performed in duplicates ± SEM (n = 6), * p < 0.05, vs UNDIFF. **(F)** Expression of CTEPHA1 and adipogenic genes in hADSCs silenced for CTEPHA1. 18S was used as housekeeping gene. Data are expressed as mean of 3 experiments each performed in duplicates ± SEM (n = 6), **p<0.01 vs siNEG.

Figure 7. Characterization of coding DE RNAs and enrichment analysis (A) Subcellular localization of deregulated genes as obtained with the NDEx database. Gene set enrichment analysis was performed on clusterProfiler R package. Gene set from Molecular Signature databases such as curated gene set (C2) and ontology gene sets (C5) and a p value cut off < 0.05 were considered for this analysis. The top 20 BP **(B)**, MF **(C)**, CC **(D)**, KEGG **(E)** and WikiPathways **(F)** enriched pathways obtained with GSEA are reported as ridge plot, where the x axis refers to the enrichment score and the color scale to the p-value. Adaptative immune response* in (B) refers to "adaptive immune response based on somatic recombination of immune receptors built from immunoglobulin superfamily domains".

Figure 8. Transcriptional characterization identifies gene signature associated with disease occurrence. DisGENET analysis shows the DE RNAs terms with an FDR ≤ 0.05 implicated in **(A)**, nutritional and metabolic diseases **(B)** immune system and **(C)** in obesity in SAT from OBF vs CTRL. The lines connecting the genes to the disease term represent the literature evidence for the terms' implication in the disease. The color scale represents the genes FC.

Supplementary Materials.

Figure S1. In silico dissection of COL4A2-AS2.

(A) COL4A2-AS2 gene locus structure as obtained from the UCSC webtool (https://genome.ucsc.edu/). **(B)** PhyloP, PhastCons and DAF scores **(C)** subcellular localization **(D)** miRNA binding sites to the lncRNAs structure (in blue) **(E)** protein binding sites to the lncRNA structure (in blue) as obtained with the AnnoLnc2 database. **(F)** COL4A2-AS2 positively correlated genes as obtained with the AnnoLnc2 database. The network was built with Cytoscape.

Figure S2. In silico dissection of RPS21-AS.

(A) RPS21-AS (AL121832.2) gene locus structure as obtained from the UCSC webtool (https://genome.ucsc.edu/). **(B)** PhyloP, PhastCons and DAF scores **(C)** subcellular localization **(D)**

miRNA binding sites to the lncRNA structure (in blue) **(E)** protein binding sites to the lncRNA structure (in blue) as obtained with the AnnoLnc2 database.

Figure S3. In silico dissection of PELATON.
(A) PELATON gene locus structure as obtained from the UCSC webtool (https://genome.ucsc.edu/). **(B)** PhyloP, PhastCons and DAF scores **(C)** subcellular localization **(D)** miRNA binding sites to the lncRNA structure (in blue) **(E)** protein binding sites to the lncRNA structure (in blue) as obtained with the AnnoLnc2 database.

Figure S4. In silico dissection of ITGB2-AS1.
(A) ITGB2-AS1 gene locus structure as obtained from the UCSC webtool (https://genome.ucsc.edu/). **(B)** PhyloP, PhastCons and DAF scores **(C)** subcellular localization **(D)** miRNA binding sites to the lncRNA structure (in blue) **(E)** protein binding sites to the lncRNA structure (in blue) as obtained with the AnnoLnc2 database.

Figure S5. In silico dissection of ACER2-AS.
(A) ACER2-AS (AL158206.1) gene locus structure as obtained from the UCSC webtool (https://genome.ucsc.edu/). **(B)** PhyloP, PhastCons and DAF scores **(C)** subcellular localization **(D)** miRNA binding sites to the lncRNA structure (in blue) **(E)** protein binding sites to the lncRNA structure (in blue) as obtained with the AnnoLnc2 database.

Figure S6. In silico dissection of CTEPHA1.
(A) CTEPHA1 (LINC01094) gene locus structure as obtained from the UCSC webtool (https://genome.ucsc.edu/). **(B)** PhyloP, PhastCons and DAF scores **(C)** subcellular localization **(D)** miRNA binding sites to the lncRNA structure (in blue) **(E)** protein binding sites to the lncRNA structure (in blue) as obtained with the AnnoLnc2 database.

Figure S7. COL4A2 and RPS21 expression during adipogenic differentiation and in presence of C/EBPβ silencing.
(A) Differential expression of COL4A2 and RPS21 in adipocytes obtained from SAT tissue from obese patients was verified by Real Time PCR. 18S was used as housekeeping gene. Data are expressed as mean of 2 samples ± SEM **(B)** Differential expression of COL4A2 and RPS21 in lipoaspirate of a CTRL subject was verified by Real Time PCR. GAPDH was used as housekeeping gene. Data are expressed as mean of 3 experiments each performed in duplicates ± SEM (n = 6), * $p < 0.05$, **$p<0.01$, vs. Day 0. **(C)**

Figure S7. Functional analysis of COL4A2 and RPS21 deregulation after C/EBPδ and C/EBPα silencing and PPARγ modulation.
(A) Differential expression of COL4A2 and RPS21 in hADSCs silenced for C/EBPβ versus control (siNEG) was verified by Real Time PCR. 18S was used as housekeeping gene. Data are expressed as mean of 3 experiments each performed in duplicates ± SEM (n = 6). **(B)** Differential expression of COL4A2 and RPS21 in hADSCs silenced for C/EBPδ versus control (siNEG) was verified by Real Time PCR. 18S was used as housekeeping gene. Data are expressed as mean of 3 experiments each performed in duplicates ± SEM (n = 6). **(C)** Differential expression of COL4A2 and RPS21 in

hADSCs silenced for C/EBPα versus control (siNEG) was verified by Real Time PCR. 18S was used as housekeeping gene. Data are expressed as mean of 3 experiments each performed in duplicates ± SEM (n = 6). **(D)** Expression of COL4A2 and RPS21 in hADSCs from healthy patients treated in undifferentiated conditions (UNDIFF), differentiated for 7 days in standard adipogenic medium (DIFF), in undifferentiated condition supplemented with Troglitazone (UNDIFF+TRO) and differentiated for 7 days in standard adipogenic medium supplemented with the PPARγ inhibitor T0070907 (DIFF + αPPARγ). Expression was verified by Real Time PCR and 18S was used as housekeeping gene. Data are expressed as mean of 3 experiments each performed in duplicates ± SEM (n = 6), * $p < 0.05$ vs UNDIFF.

Figure S8. Negative control of disease network specificity.
DisGENET analysis shows 83 randomly selected terms correlation with **(A)**, nutritional and metabolic diseases **(B)** immune system and **(C)** obesity. The lines connecting the genes to the disease term represent the literature evidence for the terms' implication in the disease.

Table S1. Clinical characteristics of patients whose SAT was analyzed in this study.

Table S2. List of Primers used.

Table S3. Repeat elements present in each lncRNA as obtained with the AnnoLnc2 database.

Table S4. Localization motifs present in each lncRNA as obtained with the AnnoLnc2 database.

Table S5. miRNAs predicted interactions with each lncRNA as obtained with the AnnoLnc2 database.

Table S6. Protein predicted interactions with each lncRNA as obtained with the AnnoLnc2 database.

Table S7. Transcription factors predicted interactions in adipocytes with each lncRNA as obtained with the AnnoLnc2 database.

Table S8. List of DE RNAs with an FDR ≤ 0.05.

Table S9. List of 83 randomly obtained genes used as negative controls for DisGeNET database analysis.

Acknowledgments

FR would like to acknowledge and thank the Fondazione Fratelli Confalonieri for financial support during her PhD. This work was supported by a grant from the Pediatric Clinical Research Center Fondazione "Romeo and Enrica Invernizzi" to GVZ and SC.

Author contributions

F.R.: Conceptualization, Data curation, Formal analysis, Writing – original draft; L.M.: Data curation, Formal analysis, Writing – original draft; C.P., B.B.: Formal analysis, Methodology; G.M.: Methodology, Resources; M.T.R., S.B., C.C.: Supervision, Writing - review & editing; R.C.: Supervision, Writing - review & editing; G.V.Z.: Resources, Supervision, Funding acquisition; S.C.: Conceptualization, Supervision, Writing - original draft.

Conflict of interest

The authors declare that they have no conflict of interest.

Author statement

F.R.: Conceptualization, Data curation, Formal analysis, Writing – original draft; L.M.: Data curation, Formal analysis, Writing – original draft; C.P., B.B.: Formal analysis, Methodology; G.M.: Methodology, Resources; M.T.R., S.B., C.C.: Supervision, Writing - review & editing; R.C.: Supervision, Writing - review & editing; G.V.Z.: Resources, Supervision, Funding acquisition; S.C.: Conceptualization, Supervision, Writing - original draft.

Highlights

- There is a crucial need to identify novel targets and players in obesity
- RNA-seq allows the analysis of subcutaneous adipose tissue dysfunctions in obesity
- Long non-coding RNAs are novel players emerging as regulators in the disease
- Differential RNA expression analysis could provide new targets altered in obesity

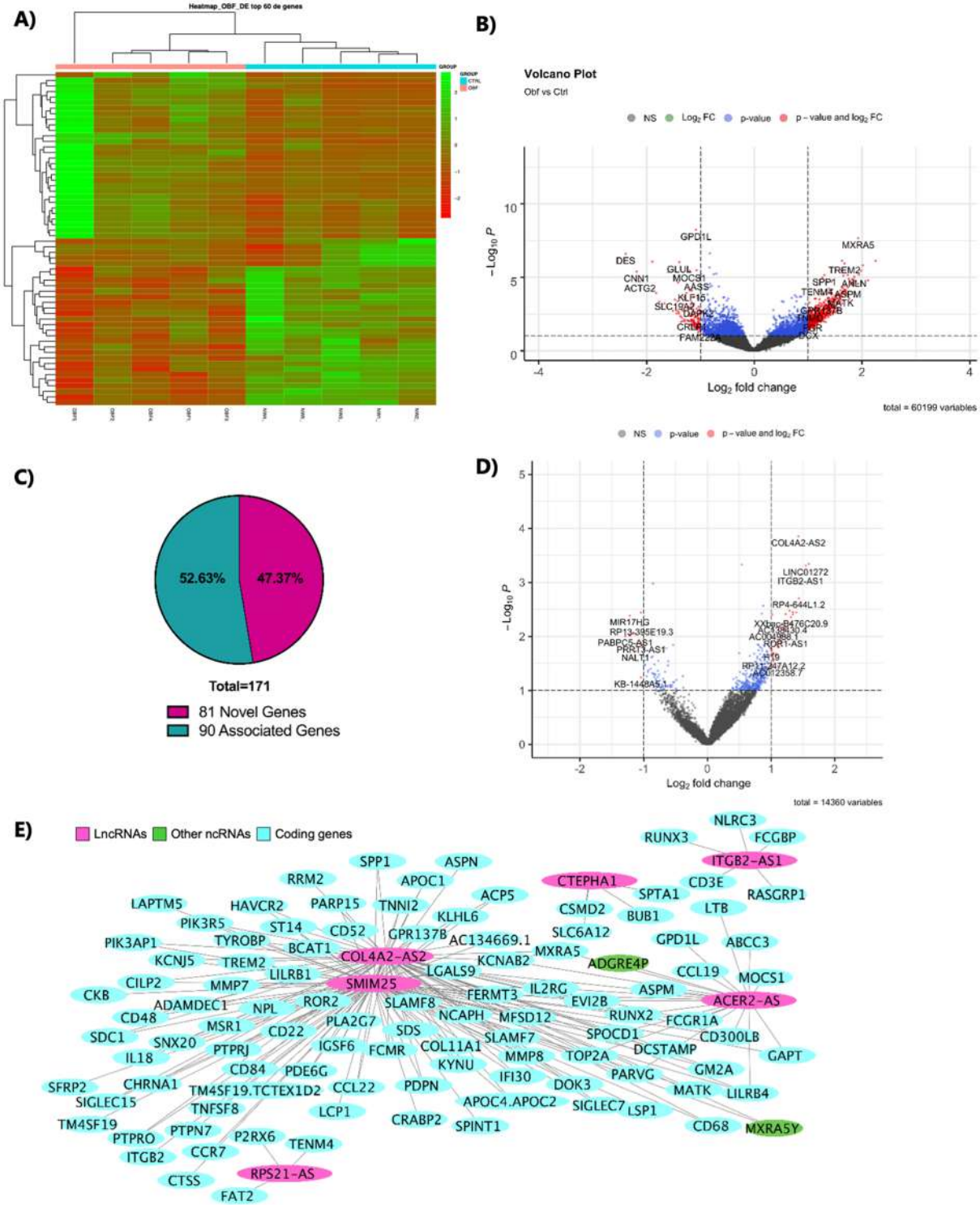
A)
Heatmap_OBF_DE top 60 de genes
GROUP
CTRL
OBF
B)
Volcano Plot
Obf vs Ctrl
NS
Log2 FC
p-value
p - value and log2 FC
−Log10 P
Log2 fold change
total = 60199 variables
GPD1L
MXRA5
DES
GLUL
TREM2
CNN1
MOCS1
SPP1
ACTG2
AASS
AHLN
KLF15
ASPM
SLC19A2
MATK
DAPK2
CRIM1
PAM22A
DCX
C)
52.63%
47.37%
Total=171
81 Novel Genes
90 Associated Genes
D)
−Log10 P
Log2 fold change
total = 14360 variables
COL4A2-AS2
LINC01272
ITGB2-AS1
RP4-644L1.2
MIR17HG
RP13-395E19.3
PABPC5-AS1
PRR13-AS1
NALT1
KB-1448A5.1
RP11-347A12.2
E)
LncRNAs
Other ncRNAs
Coding genes
SPP1
ASPN
RRM2
APOC1
LAPTM5
HAVCR2
PARP15
TNNI2
ACP5
PIK3R5
ST14
CD52
KLHL6
PIK3AP1
TYROBP
BCAT1
GPR137B
AC134669.1
KCNJ5
TREM2
COL4A2-AS2
KCNAB2
CILP2
LILRB1
LGALS9
SMIM25
MMP7
CKB
ADAMDEC1
NPL
ROR2
FERMT3
IL2RG
CD48
MSR1
PLA2G7
SLAMF8
NCAPH
MFSD12
SDC1
SNX20
CD22
SDS
SLAMF7
PTPRJ
IGSF6
COL11A1
IL18
CD84
FCMR
KYNU
MMP8
PDE6G
SFRP2
CHRNA1
TM4SF19.TCTEX1D2
CCL22
PDPN
IFI30
SIGLEC15
TNFSF8
APOC4.APOC2
TM4SF19
LCP1
CRABP2
SPINT1
PTPRO
PTPN7
P2RX6
TENM4
ITGB2
CCR7
CTSS
RPS21-AS
FAT2
CTEPHA1
CSMD2
SLC6A12
MXRA5
ADGRE4P
CD3E
SPTA1
BUB1
GPD1L
ASPM
RUNX2
SPOCD1
TOP2A
DCSTAMP
PARVG
DOK3
SIGLEC7
LSP1
NLRC3
RUNX3
FCGBP
ITGB2-AS1
RASGRP1
LTB
ABCC3
CCL19
MOCS1
ACER2-AS
FCGR1A
CD300LB
GAPT
GM2A
MATK
LILRB4
CD68
MXRA5Y

Figure 1

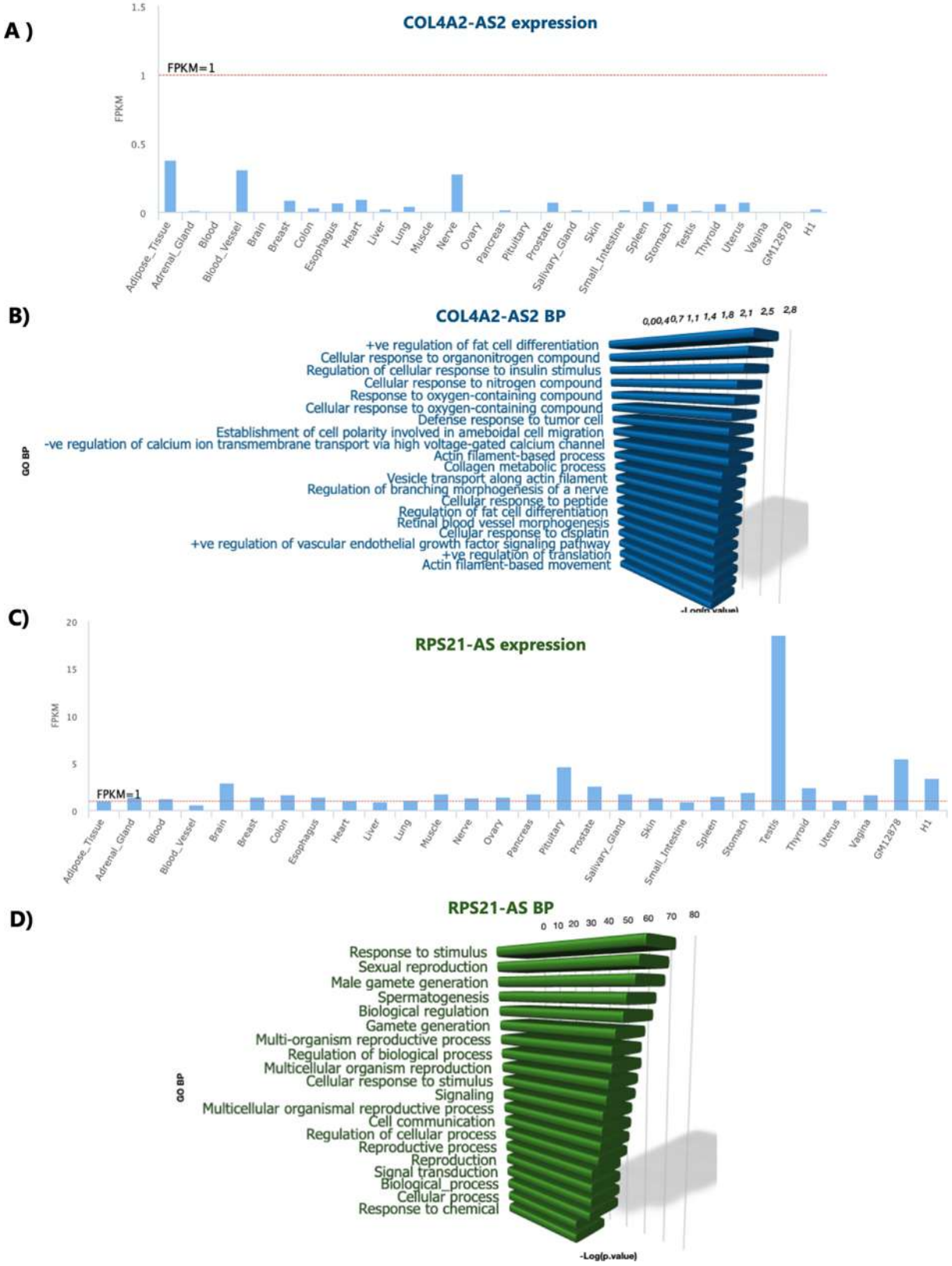
A)
COL4A2-AS2 expression
FPKM=1
FPKM
1.5
1
0.5
0
Adipose_Tissue
Adrenal_Gland
Blood
Blood_Vessel
Brain
Breast
Colon
Esophagus
Heart
Liver
Lung
Muscle
Nerve
Ovary
Pancreas
Pituitary
Prostate
Salivary_Gland
Skin
Small_Intestine
Spleen
Stomach
Testis
Thyroid
Uterus
Vagina
GM12878
H1
B)
COL4A2-AS2 BP
0,00,40,7 1,1 1,4 1,8 2,1 2,5 2,8
GO BP
+ve regulation of fat cell differentiation
Cellular response to organonitrogen compound
Regulation of cellular response to insulin stimulus
Cellular response to nitrogen compound
Response to oxygen-containing compound
Cellular response to oxygen-containing compound
Defense response to tumor cell
Establishment of cell polarity involved in ameboidal cell migration
-ve regulation of calcium ion transmembrane transport via high voltage-gated calcium channel
Actin filament-based process
Collagen metabolic process
Vesicle transport along actin filament
Regulation of branching morphogenesis of a nerve
Cellular response to peptide
Regulation of fat cell differentiation
Retinal blood vessel morphogenesis
Cellular response to cisplatin
+ve regulation of vascular endothelial growth factor signaling pathway
+ve regulation of translation
Actin filament-based movement
C)
RPS21-AS expression
FPKM
20
15
10
5
0
FPKM=1
Adipose_Tissue
Adrenal_Gland
Blood
Blood_Vessel
Brain
Breast
Colon
Esophagus
Heart
Liver
Lung
Muscle
Nerve
Ovary
Pancreas
Pituitary
Prostate
Salivary_Gland
Skin
Small_Intestine
Spleen
Stomach
Testis
Thyroid
Uterus
Vagina
GM12878
H1
D)
RPS21-AS BP
0 10 20 30 40 50 60 70 80
GO BP
Response to stimulus
Sexual reproduction
Male gamete generation
Spermatogenesis
Biological regulation
Gamete generation
Multi-organism reproductive process
Regulation of biological process
Multicellular organism reproduction
Cellular response to stimulus
Signaling
Multicellular organismal reproductive process
Cell communication
Regulation of cellular process
Reproductive process
Reproduction
Signal transduction
Biological_process
Cellular process
Response to chemical
-Log(p.value)

Figure 2

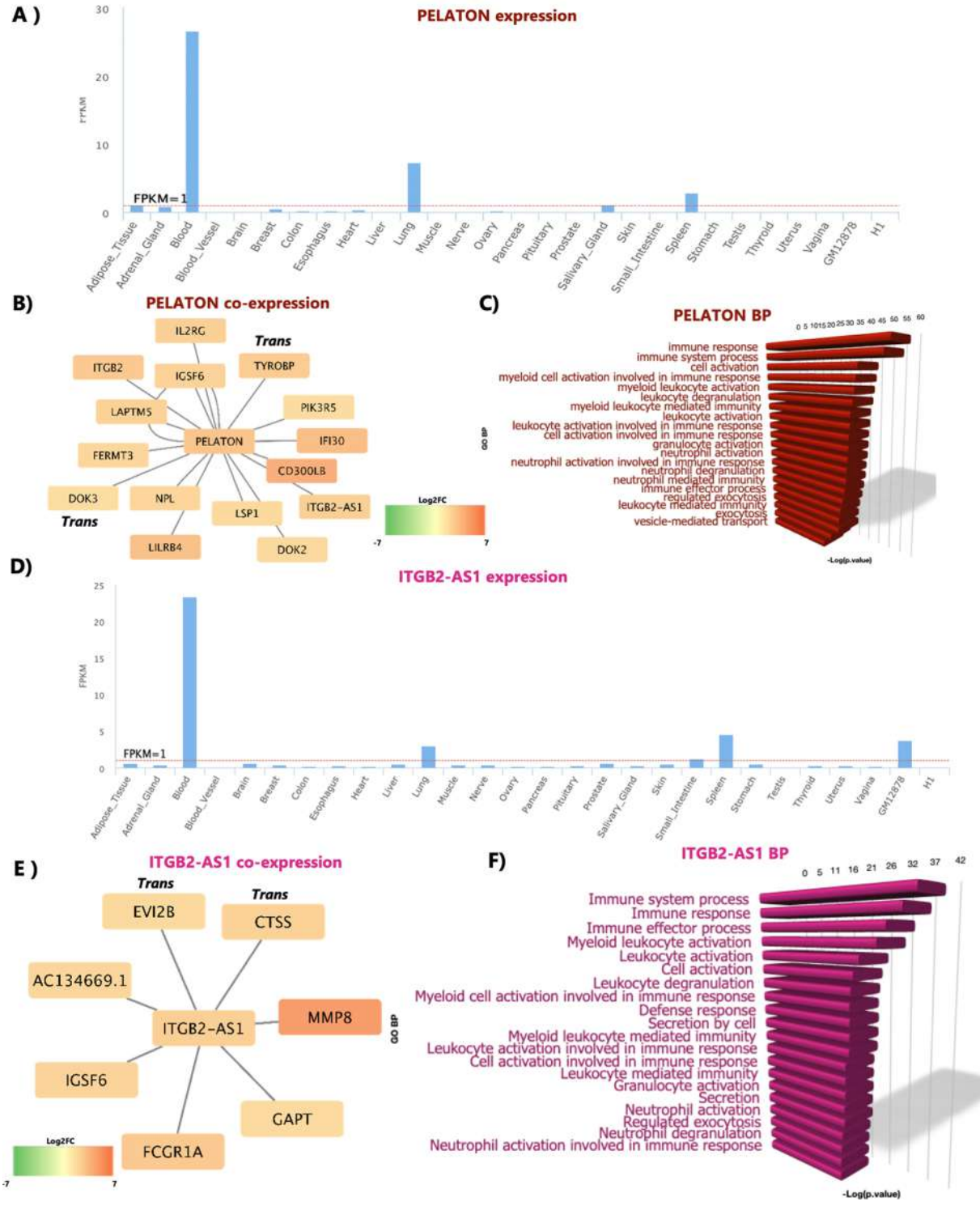
A)
PELATON expression
FPKM
FPKM=1
Adipose_Tissue
Adrenal_Gland
Blood
Blood_Vessel
Brain
Breast
Colon
Esophagus
Heart
Liver
Lung
Muscle
Nerve
Ovary
Pancreas
Pituitary
Prostate
Salivary_Gland
Skin
Small_Intestine
Spleen
Stomach
Testis
Thyroid
Uterus
Vagina
GM12878
H1
B)
PELATON co-expression
Trans
IL2RG
ITGB2
IGSF6
TYROBP
LAPTM5
PIK3R5
FERMT3
PELATON
IFI30
CD300LB
DOK3
NPL
LSP1
ITGB2-AS1
LILRB4
DOK2
Log2FC
-7
7
C)
PELATON BP
immune response
immune system process
cell activation
myeloid cell activation involved in immune response
myeloid leukocyte activation
leukocyte degranulation
myeloid leukocyte mediated immunity
leukocyte activation
leukocyte activation involved in immune response
cell activation involved in immune response
granulocyte activation
neutrophil activation
neutrophil activation involved in immune response
neutrophil degranulation
neutrophil mediated immunity
immune effector process
regulated exocytosis
leukocyte mediated immunity
exocytosis
vesicle-mediated transport
GO BP
-Log(p.value)
D)
ITGB2-AS1 expression
FPKM
FPKM=1
E)
ITGB2-AS1 co-expression
Trans
EVI2B
CTSS
AC134669.1
ITGB2-AS1
MMP8
IGSF6
GAPT
FCGR1A
Log2FC
-7
7
GO BP
F)
ITGB2-AS1 BP
Immune system process
Immune response
Immune effector process
Myeloid leukocyte activation
Leukocyte activation
Cell activation
Leukocyte degranulation
Myeloid cell activation involved in immune response
Defense response
Secretion by cell
Myeloid leukocyte mediated immunity
Leukocyte activation involved in immune response
Cell activation involved in immune response
Leukocyte mediated immunity
Granulocyte activation
Secretion
Neutrophil activation
Regulated exocytosis
Neutrophil degranulation
Neutrophil activation involved in immune response
-Log(p.value)

Figure 3

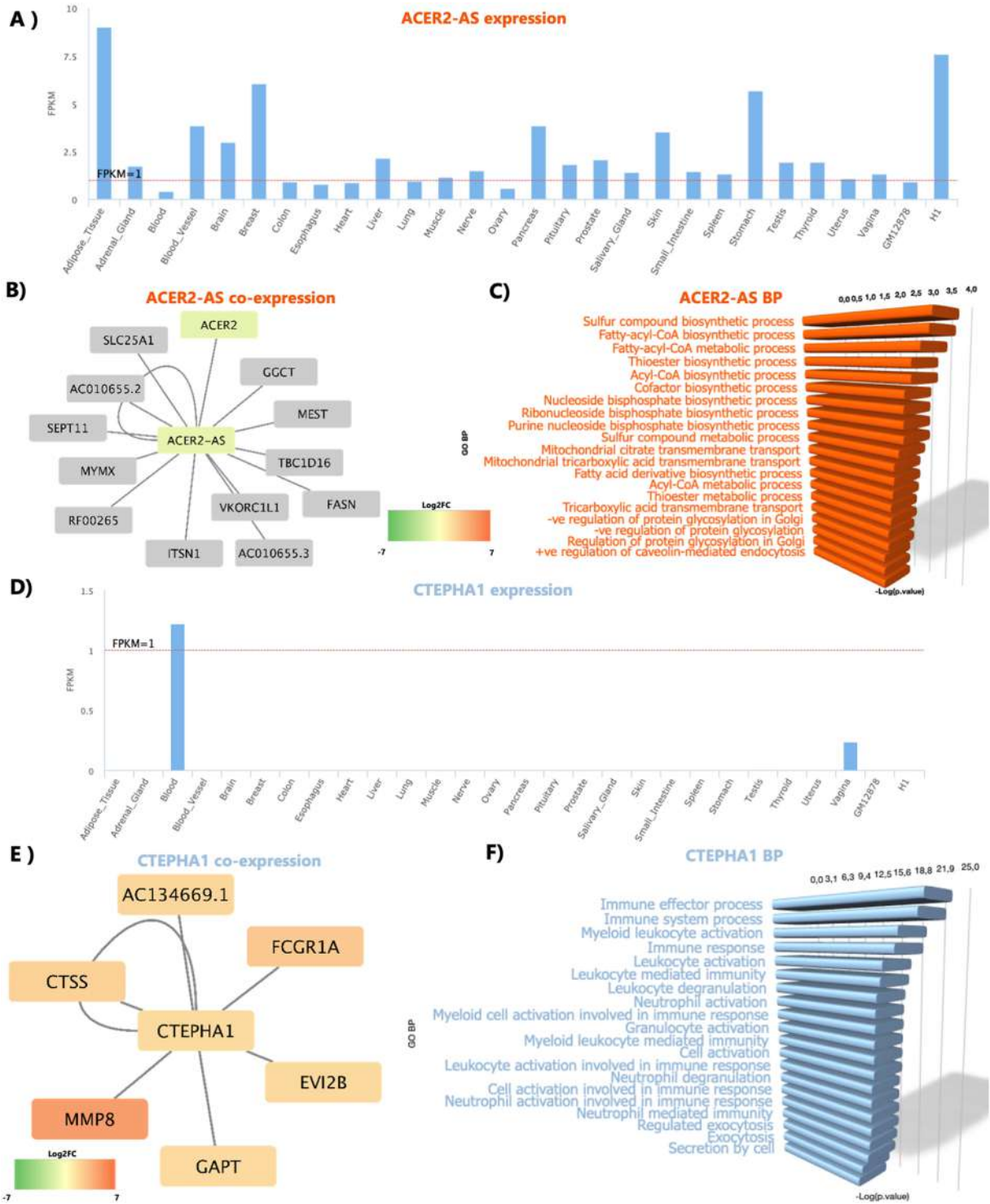
A)
ACER2-AS expression
FPKM
FPKM=1
Adipose_Tissue
Adrenal_Gland
Blood
Blood_Vessel
Brain
Breast
Colon
Esophagus
Heart
Liver
Lung
Muscle
Nerve
Ovary
Pancreas
Pituitary
Prostate
Salivary_Gland
Skin
Small_Intestine
Spleen
Stomach
Testis
Thyroid
Uterus
Vagina
GM12878
H1
B)
ACER2-AS co-expression
ACER2
SLC25A1
GGCT
AC010655.2
MEST
SEPT11
ACER2-AS
TBC1D16
MYMX
VKORC1L1
FASN
RF00265
ITSN1
AC010655.3
Log2FC
-7
7
C)
ACER2-AS BP
GO BP
Sulfur compound biosynthetic process
Fatty-acyl-CoA biosynthetic process
Fatty-acyl-CoA metabolic process
Thioester biosynthetic process
Acyl-CoA biosynthetic process
Cofactor biosynthetic process
Nucleoside bisphosphate biosynthetic process
Ribonucleoside bisphosphate biosynthetic process
Purine nucleoside bisphosphate biosynthetic process
Sulfur compound metabolic process
Mitochondrial citrate transmembrane transport
Mitochondrial tricarboxylic acid transmembrane transport
Fatty acid derivative biosynthetic process
Acyl-CoA metabolic process
Thioester metabolic process
Tricarboxylic acid transmembrane transport
-ve regulation of protein glycosylation in Golgi
-ve regulation of protein glycosylation
Regulation of protein glycosylation in Golgi
+ve regulation of caveolin-mediated endocytosis
-Log(p.value)
D)
CTEPHA1 expression
FPKM
FPKM=1
E)
CTEPHA1 co-expression
AC134669.1
FCGR1A
CTSS
CTEPHA1
EVI2B
MMP8
GAPT
Log2FC
-7
7
F)
CTEPHA1 BP
GO BP
Immune effector process
Immune system process
Myeloid leukocyte activation
Immune response
Leukocyte activation
Leukocyte mediated immunity
Leukocyte degranulation
Neutrophil activation
Myeloid cell activation involved in immune response
Granulocyte activation
Myeloid leukocyte mediated immunity
Cell activation
Leukocyte activation involved in immune response
Neutrophil degranulation
Cell activation involved in immune response
Neutrophil activation involved in immune response
Neutrophil mediated immunity
Regulated exocytosis
Exocytosis
Secretion by cell
-Log(p.value)

Figure 4

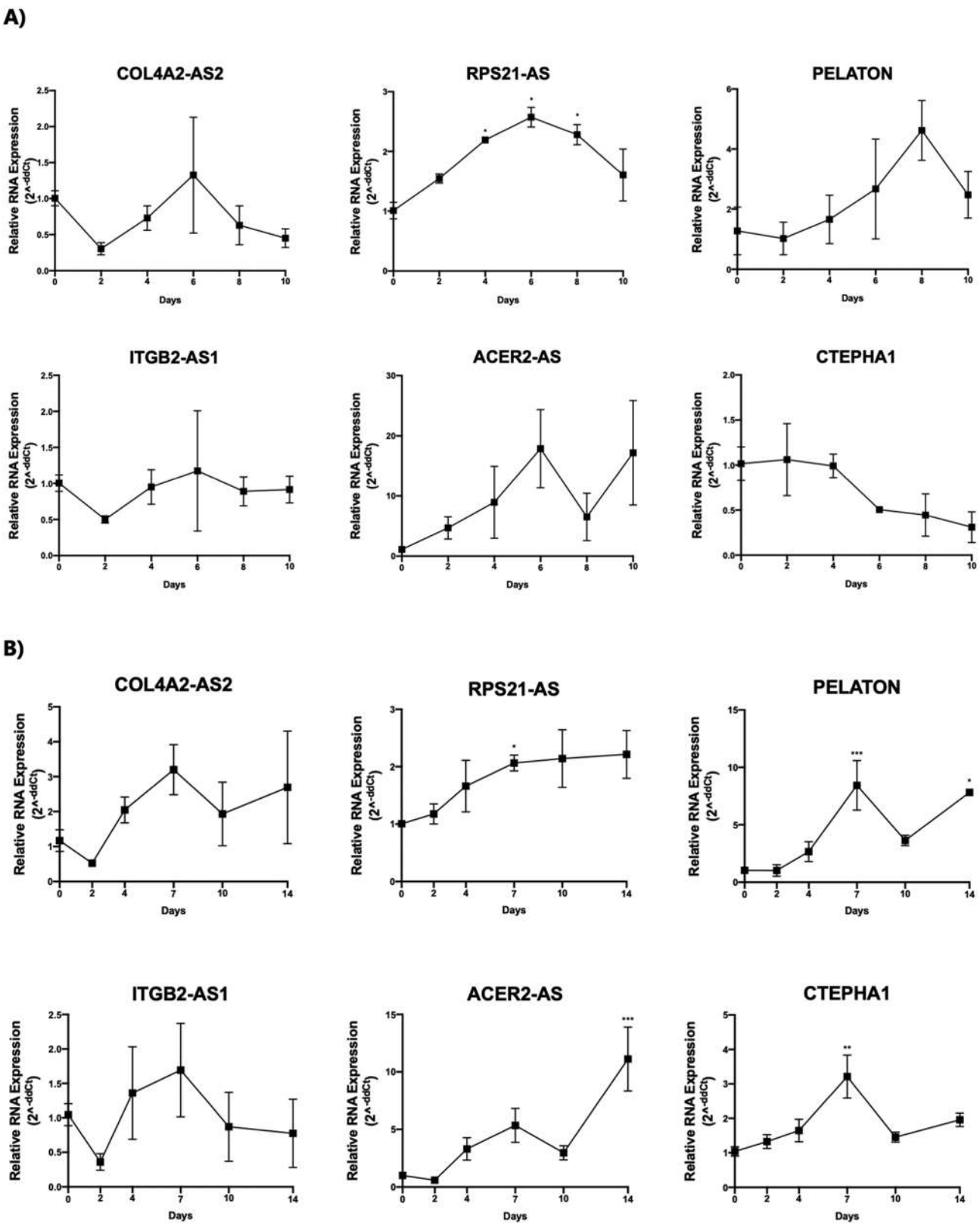
A)
COL4A2-AS2
RPS21-AS
PELATON
ITGB2-AS1
ACER2-AS
CTEPHA1
B)
COL4A2-AS2
RPS21-AS
PELATON
ITGB2-AS1
ACER2-AS
CTEPHA1
Relative RNA Expression (2^-ddCt)
Days

Figure 5

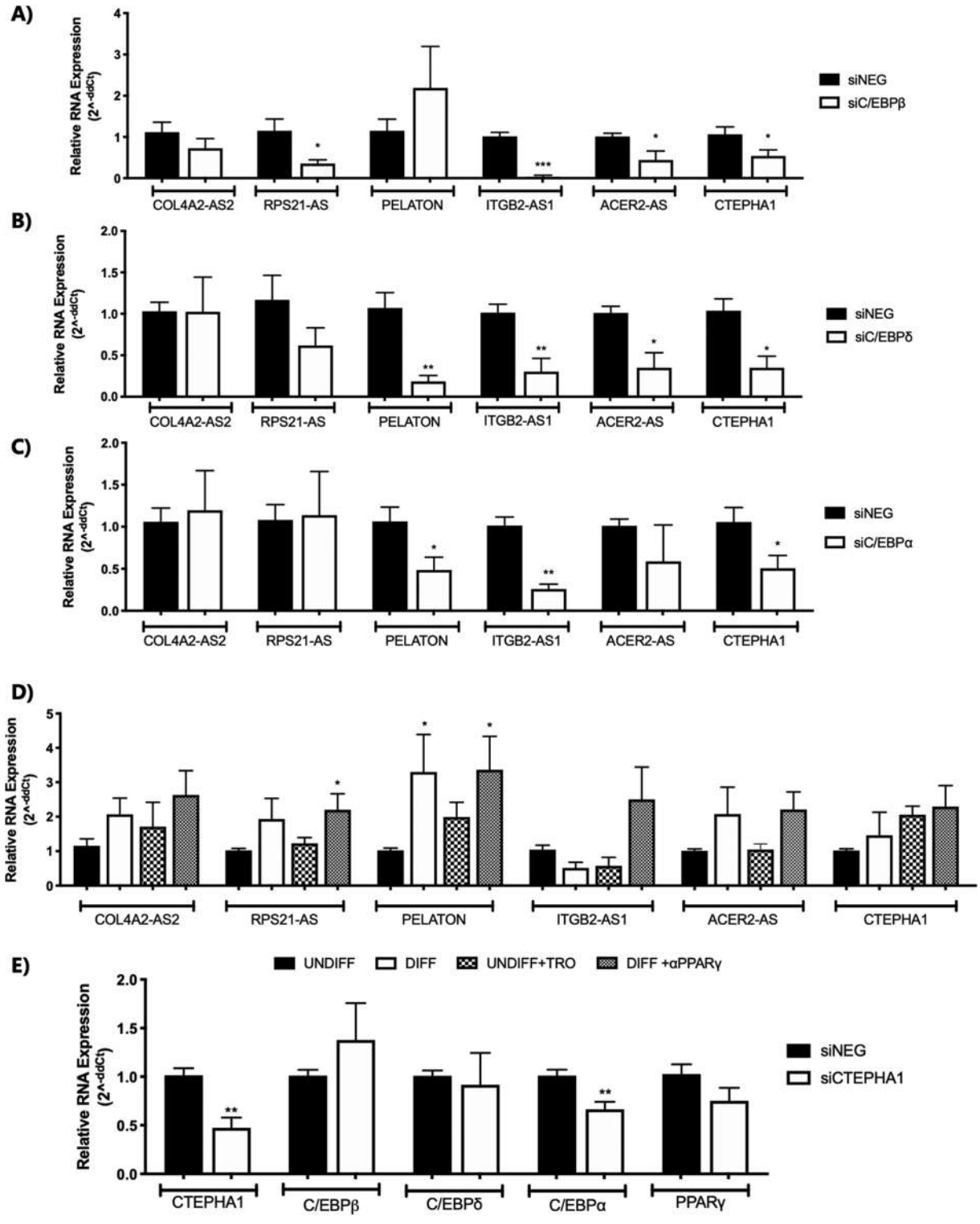
A)
Relative RNA Expression (2^-ddCt)
siNEG
siC/EBPβ
COL4A2-AS2
RPS21-AS
PELATON
ITGB2-AS1
ACER2-AS
CTEPHA1
B)
Relative RNA Expression (2^-ddCt)
siNEG
siC/EBPδ
C)
Relative RNA Expression (2^-ddCt)
siNEG
siC/EBPα
D)
Relative RNA Expression (2^-ddCt)
UNDIFF
DIFF
UNDIFF+TRO
DIFF +αPPARγ
E)
Relative RNA Expression (2^-ddCt)
siNEG
siCTEPHA1
CTEPHA1
C/EBPβ
C/EBPδ
C/EBPα
PPARγ

Figure 6

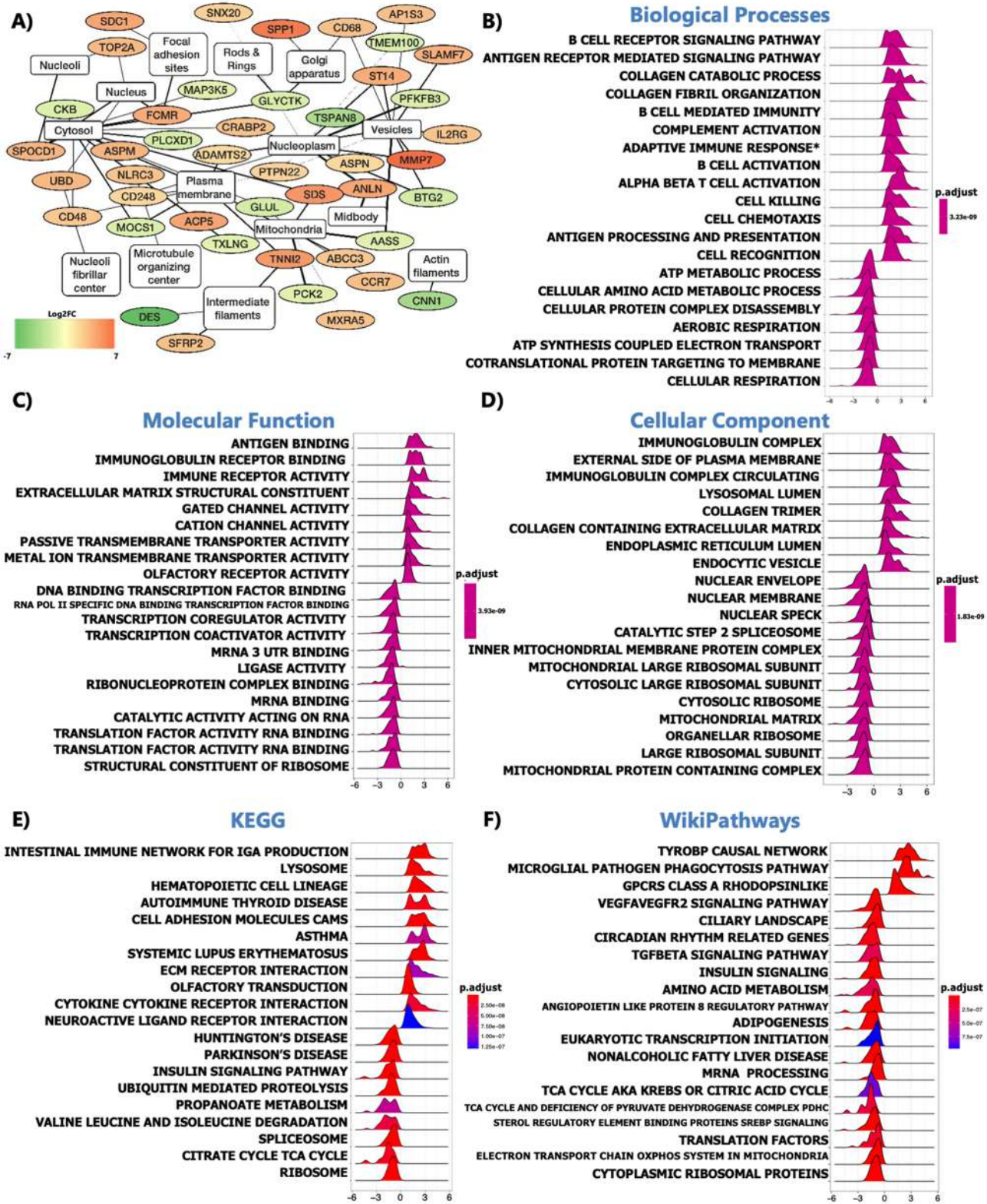
A)
SDC1
SNX20
AP1S3
SPP1
CD68
TOP2A
Focal adhesion sites
Rods & Rings
TMEM100
SLAMF7
Nucleoli
Golgi apparatus
ST14
Nucleus
MAP3K5
GLYCTK
PFKFB3
CKB
FCMR
TSPAN8
Cytosol
CRABP2
Vesicles
IL2RG
PLCXD1
Nucleoplasm
SPOCD1
ASPM
ADAMTS2
ASPN
MMP7
UBD
NLRC3
PTPN22
Plasma membrane
SDS
ANLN
BTG2
CD248
GLUL
CD48
Midbody
MOCS1
ACP5
Mitochondria
TXLNG
AASS
Nucleoli fibrillar center
Microtubule organizing center
TNNI2
ABCC3
Actin filaments
CCR7
PCK2
CNN1
Intermediate filaments
Log2FC
DES
MXRA5
SFRP2
-7
7
B)
Biological Processes
B CELL RECEPTOR SIGNALING PATHWAY
ANTIGEN RECEPTOR MEDIATED SIGNALING PATHWAY
COLLAGEN CATABOLIC PROCESS
COLLAGEN FIBRIL ORGANIZATION
B CELL MEDIATED IMMUNITY
COMPLEMENT ACTIVATION
ADAPTIVE IMMUNE RESPONSE*
B CELL ACTIVATION
ALPHA BETA T CELL ACTIVATION
CELL KILLING
CELL CHEMOTAXIS
ANTIGEN PROCESSING AND PRESENTATION
CELL RECOGNITION
ATP METABOLIC PROCESS
CELLULAR AMINO ACID METABOLIC PROCESS
CELLULAR PROTEIN COMPLEX DISASSEMBLY
AEROBIC RESPIRATION
ATP SYNTHESIS COUPLED ELECTRON TRANSPORT
COTRANSLATIONAL PROTEIN TARGETING TO MEMBRANE
CELLULAR RESPIRATION
p.adjust
3.23e-09
-6 -3 0 3 6
C)
Molecular Function
ANTIGEN BINDING
IMMUNOGLOBULIN RECEPTOR BINDING
IMMUNE RECEPTOR ACTIVITY
EXTRACELLULAR MATRIX STRUCTURAL CONSTITUENT
GATED CHANNEL ACTIVITY
CATION CHANNEL ACTIVITY
PASSIVE TRANSMEMBRANE TRANSPORTER ACTIVITY
METAL ION TRANSMEMBRANE TRANSPORTER ACTIVITY
OLFACTORY RECEPTOR ACTIVITY
DNA BINDING TRANSCRIPTION FACTOR BINDING
RNA POL II SPECIFIC DNA BINDING TRANSCRIPTION FACTOR BINDING
TRANSCRIPTION COREGULATOR ACTIVITY
TRANSCRIPTION COACTIVATOR ACTIVITY
MRNA 3 UTR BINDING
LIGASE ACTIVITY
RIBONUCLEOPROTEIN COMPLEX BINDING
MRNA BINDING
CATALYTIC ACTIVITY ACTING ON RNA
TRANSLATION FACTOR ACTIVITY RNA BINDING
TRANSLATION FACTOR ACTIVITY RNA BINDING
STRUCTURAL CONSTITUENT OF RIBOSOME
p.adjust
3.93e-09
-6 -3 0 3 6
D)
Cellular Component
IMMUNOGLOBULIN COMPLEX
EXTERNAL SIDE OF PLASMA MEMBRANE
IMMUNOGLOBULIN COMPLEX CIRCULATING
LYSOSOMAL LUMEN
COLLAGEN TRIMER
COLLAGEN CONTAINING EXTRACELLULAR MATRIX
ENDOPLASMIC RETICULUM LUMEN
ENDOCYTIC VESICLE
NUCLEAR ENVELOPE
NUCLEAR MEMBRANE
NUCLEAR SPECK
CATALYTIC STEP 2 SPLICEOSOME
INNER MITOCHONDRIAL MEMBRANE PROTEIN COMPLEX
MITOCHONDRIAL LARGE RIBOSOMAL SUBUNIT
CYTOSOLIC LARGE RIBOSOMAL SUBUNIT
CYTOSOLIC RIBOSOME
MITOCHONDRIAL MATRIX
ORGANELLAR RIBOSOME
LARGE RIBOSOMAL SUBUNIT
MITOCHONDRIAL PROTEIN CONTAINING COMPLEX
p.adjust
1.83e-09
-3 0 3 6
E)
KEGG
INTESTINAL IMMUNE NETWORK FOR IGA PRODUCTION
LYSOSOME
HEMATOPOIETIC CELL LINEAGE
AUTOIMMUNE THYROID DISEASE
CELL ADHESION MOLECULES CAMS
ASTHMA
SYSTEMIC LUPUS ERYTHEMATOSUS
ECM RECEPTOR INTERACTION
OLFACTORY TRANSDUCTION
CYTOKINE CYTOKINE RECEPTOR INTERACTION
NEUROACTIVE LIGAND RECEPTOR INTERACTION
HUNTINGTON'S DISEASE
PARKINSON'S DISEASE
INSULIN SIGNALING PATHWAY
UBIQUITIN MEDIATED PROTEOLYSIS
PROPANOATE METABOLISM
VALINE LEUCINE AND ISOLEUCINE DEGRADATION
SPLICEOSOME
CITRATE CYCLE TCA CYCLE
RIBOSOME
p.adjust
2.50e-08
5.00e-08
7.50e-08
1.00e-07
1.25e-07
-6 -3 0 3 6
F)
WikiPathways
TYROBP CAUSAL NETWORK
MICROGLIAL PATHOGEN PHAGOCYTOSIS PATHWAY
GPCRS CLASS A RHODOPSINLIKE
VEGFAVEGFR2 SIGNALING PATHWAY
CILIARY LANDSCAPE
CIRCADIAN RHYTHM RELATED GENES
TGFBETA SIGNALING PATHWAY
INSULIN SIGNALING
AMINO ACID METABOLISM
ANGIOPOIETIN LIKE PROTEIN 8 REGULATORY PATHWAY
ADIPOGENESIS
EUKARYOTIC TRANSCRIPTION INITIATION
NONALCOHOLIC FATTY LIVER DISEASE
MRNA PROCESSING
TCA CYCLE AKA KREBS OR CITRIC ACID CYCLE
TCA CYCLE AND DEFICIENCY OF PYRUVATE DEHYDROGENASE COMPLEX PDHC
STEROL REGULATORY ELEMENT BINDING PROTEINS SREBP SIGNALING
TRANSLATION FACTORS
ELECTRON TRANSPORT CHAIN OXPHOS SYSTEM IN MITOCHONDRIA
CYTOPLASMIC RIBOSOMAL PROTEINS
p.adjust
2.5e-07
5.0e-07
7.5e-07
-6 -3 0 3 6

Figure 7

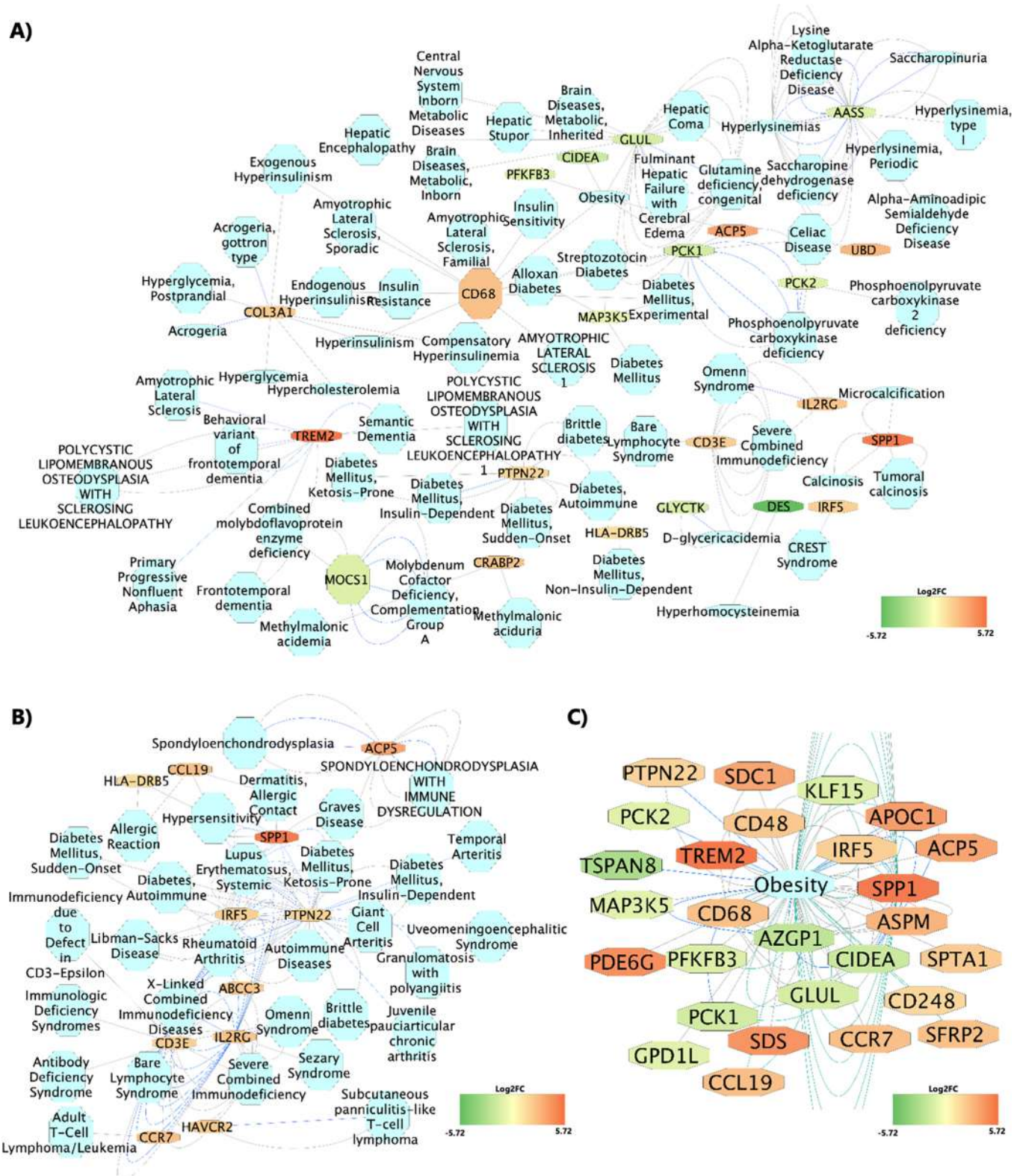
A)
Lysine Alpha-Ketoglutarate Reductase Deficiency Disease
Saccharopinuria
Central Nervous System Inborn Metabolic Diseases
Hepatic Stupor
Brain Diseases, Metabolic, Inherited
Hepatic Coma
AASS
Hyperlysinemia, type I
Hepatic Encephalopathy
GLUL
Hyperlysinemias
Hyperlysinemia, Periodic
Exogenous Hyperinsulinism
Brain Diseases, Metabolic, Inborn
CIDEA
PFKFB3
Fulminant Hepatic Failure with Cerebral Edema
Glutamine deficiency, congenital
Saccharopine dehydrogenase deficiency
Obesity
Alpha-Aminoadipic Semialdehyde Deficiency Disease
Amyotrophic Lateral Sclerosis, Sporadic
Insulin Sensitivity
Amyotrophic Lateral Sclerosis, Familial
ACP5
Celiac Disease
Acrogeria, gottron type
PCK1
UBD
Streptozotocin Diabetes
Hyperglycemia, Postprandial
Endogenous Hyperinsulinism
Insulin Resistance
CD68
Alloxan Diabetes
PCK2
Phosphoenolpyruvate carboxykinase 2 deficiency
Diabetes Mellitus, Experimental
COL3A1
MAP3K5
Acrogeria
Phosphoenolpyruvate carboxykinase deficiency
Hyperinsulinism
Compensatory Hyperinsulinemia
AMYOTROPHIC LATERAL SCLEROSIS 1
Diabetes Mellitus
Omenn Syndrome
Amyotrophic Lateral Sclerosis
Hyperglycemia
Hypercholesterolemia
POLYCYSTIC LIPOMEMBRANOUS OSTEODYSPLASIA WITH SCLEROSING LEUKOENCEPHALOPATHY 1
IL2RG
Microcalcification
Behavioral variant of frontotemporal dementia
TREM2
Semantic Dementia
Brittle diabetes
Bare Lymphocyte Syndrome
CD3E
Severe Combined Immunodeficiency
SPP1
POLYCYSTIC LIPOMEMBRANOUS OSTEODYSPLASIA WITH SCLEROSING LEUKOENCEPHALOPATHY
Diabetes Mellitus, Ketosis-Prone
PTPN22
Calcinosis
Tumoral calcinosis
Diabetes Mellitus, Insulin-Dependent
Diabetes, Autoimmune
GLYCTK
DES
IRF5
Combined molybdoflavoprotein enzyme deficiency
Diabetes Mellitus, Sudden-Onset
HLA-DRB5
D-glycericacidemia
CREST Syndrome
Primary Progressive Nonfluent Aphasia
MOCS1
Molybdenum Cofactor Deficiency, Complementation Group A
CRABP2
Diabetes Mellitus, Non-Insulin-Dependent
Frontotemporal dementia
Methylmalonic aciduria
Hyperhomocysteinemia
Methylmalonic acidemia
Log2FC
-5.72
5.72
B)
Spondyloenchondrodysplasia
ACP5
CCL19
SPONDYLOENCHONDRODYSPLASIA WITH IMMUNE DYSREGULATION
HLA-DRB5
Dermatitis, Allergic Contact
Hypersensitivity
Graves Disease
Diabetes Mellitus, Sudden-Onset
Allergic Reaction
SPP1
Temporal Arteritis
Lupus Erythematosus, Systemic
Diabetes Mellitus, Ketosis-Prone
Diabetes Mellitus, Insulin-Dependent
Diabetes, Autoimmune
Immunodeficiency due to Defect in CD3-Epsilon
IRF5
PTPN22
Giant Cell Arteritis
Uveomeningoencephalitic Syndrome
Libman-Sacks Disease
Rheumatoid Arthritis
Autoimmune Diseases
Granulomatosis with polyangiitis
Immunologic Deficiency Syndromes
X-Linked Combined Immunodeficiency Diseases
ABCC3
Brittle diabetes
Juvenile pauciarticular chronic arthritis
Omenn Syndrome
CD3E
IL2RG
Antibody Deficiency Syndrome
Bare Lymphocyte Syndrome
Severe Combined Immunodeficiency
Sezary Syndrome
Subcutaneous panniculitis-like T-cell lymphoma
Adult T-Cell Lymphoma/Leukemia
CCR7
HAVCR2
Log2FC
-5.72
5.72
C)
PTPN22
SDC1
KLF15
PCK2
CD48
APOC1
TREM2
IRF5
ACP5
TSPAN8
Obesity
SPP1
MAP3K5
CD68
ASPM
AZGP1
PDE6G
PFKFB3
CIDEA
SPTA1
GLUL
CD248
PCK1
SDS
CCR7
SFRP2
GPD1L
CCL19
Log2FC
-5.72
5.72

Figure 8